https://doi.org/10.1016/j.ejmech.2018.12.063

Design, Biological Evaluation and X-ray Crystallography of Nanomolar Multifunctional Ligands Targeting Simultaneously Acetylcholinesterase and Glycogen Synthase Kinase-3

Killian Oukoloff,[a] Nicolas Coquelle, [b,c] Manuela Bartolini,[d] Marina Naldi,[d] Rémy Le Guevel,[e] Stéphane Bach,[f] Béatrice Josselin [f] Sandrine Ruchaud,[f] Marco Catto,[g] Leonardo Pisani,[g] Nunzio Denora,[g] Rosa Maria Iacobazzi,[h] Israel Silman,[i] Joel L. Sussman,[j] Frédéric Buron,[k] Jacques-Philippe Colletier,[b] Ludovic Jean,[*,a] Sylvain Routier,[k] and Pierre-Yves Renard[*,a]

[a] Normandie Univ, UNIROUEN, INSA Rouen, CNRS, COBRA (UMR 6014), 76000 Rouen, France

[b] Institut de Biologie Structurale, Université Grenoble Alpes, Centre National de la Recherche Scientifique (CNRS)-Commissariat à l'Énergie Atomique (CEA) (UMR 5075), F-38054 Grenoble, France

[c] Institut Laue Langevin, 71, avenue des Martyrs - CS 20156, 38042 Grenoble cedex 9, France

[d] Department of Pharmacy and Biotechnology, Alma Mater Studiorum University of Bologna, Via Belmeloro 6, I-40126, Bologna, Italy

[e] Plateforme ImPACcell-SFR BIOSIT UMS-CNRS3480 UMS-INSERM018, Université de Rennes1, 35043, Rennes Cedex, France

[f] Sorbonne Université, CNRS USR 3151, Protein Phosphorylation & Human Diseases, Station Biologique de Roscoff, CS 90074, Roscoff Cedex F-29688, France

[g] Dipartimento di Farmacia-Scienze del Farmaco, Università degli Studi di Bari "Aldo Moro", via Edoardo Orabona 4, 70125 Bari, Italy

[h] Istituto Tumori IRCCS Giovanni Paolo II, via le Orazio Flacco 65, 70124 Bari, Italy

[i] Department of Neurobiology, Weizmann Institute of Science, 6100 Rehovot, Israel

[j] Department of Structural Biology, Weizmann Institute of Science, 76100 Rehovot, Israel

[k] Institut de Chimie Organique et Analytique, Université d'Orléans, UMR CNRS 7311, rue de Chartres, BP 6759, 45067 Orléans Cedex 2, France

Corresponding Author

* For L. J.: phone: +33 2 35 52 24 51; E-mail: ludovic.jean@univ-rouen.fr

* For P.-Y. R.: phone: +33 2 35 52 24 76; E-mail: pierre-yves.renard@univ-rouen.fr.

Keywords

Alzheimer's disease, acetylcholinesterase, butyrylcholinesterase, kinases, glycogen synthase kinase-3, cyclin-dependent kinase 5, synthesis, SAR, crystallography.

Abstract

Both cholinesterases (AChE and BChE) and kinases, such as GSK-3α/β, are associated with the pathology of Alzheimer's disease. Two scaffolds, targeting AChE and GSK-3α/β simultaneously, were assembled, using copper(I)-catalysed azide alkyne cycloaddition (CuAAC), to generate a new series of multifunctional ligands. A series of eight multi-target directed ligands (MTDLs) was synthesized and evaluated *in vitro* and in cell cultures. Molecular docking studies, together with the crystal structures of three MTDL/*Tc*AChE complexes, with three tacrine-valmerin hybrids allowed designing an appropriate linker containing a 1,2,3-triazole moiety whose incorporation preserved, and even increased, the original inhibitory potencies of the two selected pharmacophores toward the two targets. Most of the new derivatives exhibited nanomolar affinity for both targets, and the most potent compound of the series displayed inhibitory potencies of 9.5 nM for human acetylcholinesterase (hAChE) and 7 nM for GSK-3α/β. These novel dual MTDLs may serve as suitable leads for further development, since, in the micromolar range, they exhibited low cytotoxicity on a panel of representative human cell lines including the human neuroblastoma cell line SH-SY5Y. Moreover, these tacrine-valmerin

hybrids displayed a good ability to penetrate the blood-brain barrier (BBB) without interacting with efflux pumps such as P-gp.

1. Introduction

Alzheimer's disease (AD), the most common cause of senile dementia, is a major public health concern with devastating social impact. In 2016, Alzheimer's Disease International, the worldwide federation of Alzheimer associations, estimated that 47 million people were affected by this type of dementia, and predicted that 131 million people will be affected in 2050. Thus, the economic impact of the disease on future long-term care costs will be enormous. Already in 2018 the cost of treatment of dementia is estimated to reach US$ 1 trillion, rising to US$ 2 trillion by 2030.[1]

AD results from a neurodegenerative process occurring in the central nervous system (CNS). It is clinically characterized by loss of memory and cognitive impairment, which parallel the deterioration of cholinergic neurons in the basal-forebrain with concurrent reduced levels of the neurotransmitter acetylcholine (ACh). The disease is histologically characterized by extracellular deposits of β-amyloid peptide (Aβ) and intracellular formation of neurofibrillary tangles (NFTs).[2, 3] Other hallmarks include oxidative stress, dys-homeostasis of biometals and calcium, inflammation and loss of synaptic connections.[4] Current therapeutic options for treatment of AD mostly aim at restoring physiological ACh level by inhibiting the enzyme acetylcholinesterase (AChE) which is responsible for the hydrolysis of ACh. Therefore, three drugs approved by the Food and Drug administration (FDA) for the management of AD are AChE inhibitors (AChEIs), namely donepezil, rivastigmine and galantamine.[5] However, treatment with AChEIs is mostly symptomatic and effective only for AD patients with mild-to-moderate symptoms, enabling in some cases the progression of cognitive and functional

impairments to be retarded. Memantine, which is an *N*-methyl-D-aspartate (NMDA) receptor antagonist, is the latest drug approved for the treatment of the disease.[6] The efficacy of memantine is similar to that of the AChEIs among patients with mild-to-moderate symptoms, but has been reported to be more useful for treating patients at more advanced stages of the disease.[7-9] Yet, all four drugs only provide temporary symptomatic relief, but do not provide a cure. Despite efforts over the last few decades of both academic research teams and pharmaceutical companies, no curative treatment has emerged yet.[10-12]

An attrition factor to the development of curative drugs is the fact that the aetiology of AD is not fully understood. It is recognized, however, that the processes resulting in its development and progression are complex and multifactorial.[13] Thus, it is conceivable to hypothesize that a combination of synergetic strategies targeting the various players involved in the onset and development of the disease should be more beneficial and should present a higher rate of success. The "multifactorial hypothesis" has fuelled the so-called multi-target-directed ligand (MTDL) strategy which foresees the development of a single molecule able to hit several key targets/pathways.[14-22] Besides the advantage of acting simultaneously on more than one biological target, MTDLs have the advantages of a higher patient compliance (a parameter of paramount importance for such neurodegenerative disease), lower risk of drug-drug interactions, and lower costs to perform ADMET studies.[23]

Kinases have been shown to be associated with the progression of AD, and have received increased attention during the past decade.[24, 25] Some members of this family are involved in the hyperphosphorylation of the tau protein, which results in the production of intracellular NFTs. GSK-3β [26] and CDK5 [27] are the two main kinases involved in this process, whereas GSK-3α appears to regulate the production of Aβ.[28, 29] Thus, GSK inhibitors may be useful

for treatment of AD, as well as of other neurodegenerative diseases.[30, 31] A study identified novel mechanisms linking GSK-3 with the Aβ pathology. The inhibition of GSK-3 reversed AD pathogenesis *via* lysosomal acidification and reactivation restoration of the mammalian target of rapamycin (mTOR) in a mouse model of AD.[32] Furthermore, evidence has been presented that GSK-3 inhibitors may reduce Aβ-oligomer-induced neuronal toxicity and may promote neurogenesis *in vitro* and *in vivo.*[33, 34] These various studies indicate that GSK-3 inhibitors should be further studied as candidates for treatment of AD.[35]

A renewed interest in AChEIs for AD treatment arose when evidence was presented that in addition to AChE inhibition, certain AChEIs may block the involvement of AChE in mediating the aggregation and deposition of Aβ peptides.[36-38] Thus, AChE has been reported to accelerate the formation of neurotoxic Aβ aggregates *via* a mechanism that involves its peripheral anionic site (PAS).[39] This resulted in numerous studies aimed at developing dual binding site AChEIs interacting with both the catalytic site and the PAS.[21, 40, 41] Moreover, recent studies have suggested a possible role for AChE in hyperphosphorylated tau (P-Tau) dysregulation.[42] There is thus also a great interest in developing MTDLs endowed with an anti-ChE activity.

To combine the beneficial effect of ChE inhibition and GSK-3 inhibition within a single molecule, tacrine scaffold was selected to grant activity toward ChEs (Figure 1). This selection is also based on the fact that tacrine pharmacophore can easily be substituted on its primary amino group while retaining a satisfactory anticholinesterase activity. Consequently, many tacrine-based MTDLs exhibiting high affinity for AChE and/or BChE have been reported in the past decade.[41, 43-45] Only one example of GSK-3/AChE bifunctional inhibitors was recently

reported.[46] These MDTLs presented good inhibitory activities towards both enzymes and alleviated cognitive impairment in the mouse model treated with scopolamine.

Amongst the GSK-3 kinase inhibitors developed for application to the CNS,[47] we selected the valmerins (Figure 1), which contain a tetrahydropyrido[1,2-*a*]isoindolone core[48, 49] linked to an heteroaryl moiety by a ureido group. The pharmacophore that interacts with the kinase active site consists of the isoindolone-urea moiety linked to the pyridine ring at its C-2' position.

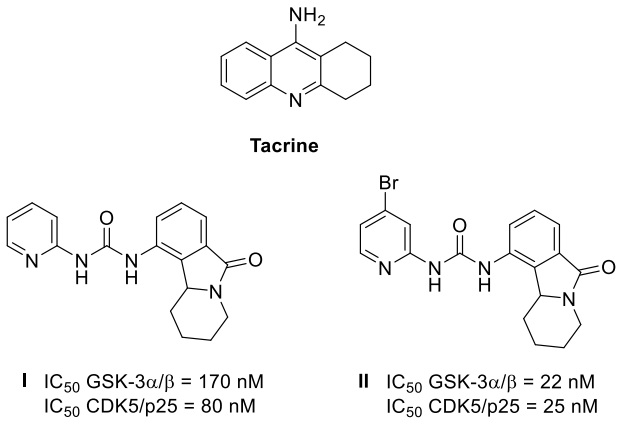

Figure 1. Structures of tacrine as ChEs inhibitor and valmerins I and II, which display potent CDK5 and GSK-3α/β inhibition activity.[49]

Docking studies and SAR studies suggested that substitutions on pyridine C4', C5' and C6' positions should not adversely affect affinity for either GSK-3α/β or CDK5. Indeed, as seen in Fig. 2, the presence of a bromine atom on C4' actually enhances inhibitory capacity several fold.[49] Thus, effective valmerin/tacrine MTDLs could be obtained using either of these positions to link the two functional groups. Linkage of the two pharmacophores could be advantageously performed using the copper(I)-catalysed azide alkyne cycloaddition (CuAAC) (Figure 2) as an interesting convergent synthetic strategy of MTDLs. Furthermore, the introduction of a 1,2,3-triazole ring within the linker connecting the two pharmacophores would allow formation of favourable hydrogen bond interactions within the active-site gorge of

AChE.[50-52] Since, the crystal structure of the complex of mouse AChE with one of the most active bifunctional AChEI, *anti*-TZ2-PA6 (PDB 1Q84), that contains a triazole ring attached to a tacrine moiety through a two-carbon linker, revealed additional hydrogen bonds between the triazole moiety and well identified residues.[50] Taking these different factors into consideration, we designed a series of MTDLs based on the skeleton depicted in Figure 2. These hybrids present a single chiral centre on the tetrahydroisoindolone moiety. Since this moiety could potentially interact with both of the targeted enzymes, for the most promising derivatives, each enantiomer was synthesized and evaluated independently for the candidate MTDLs synthesized.

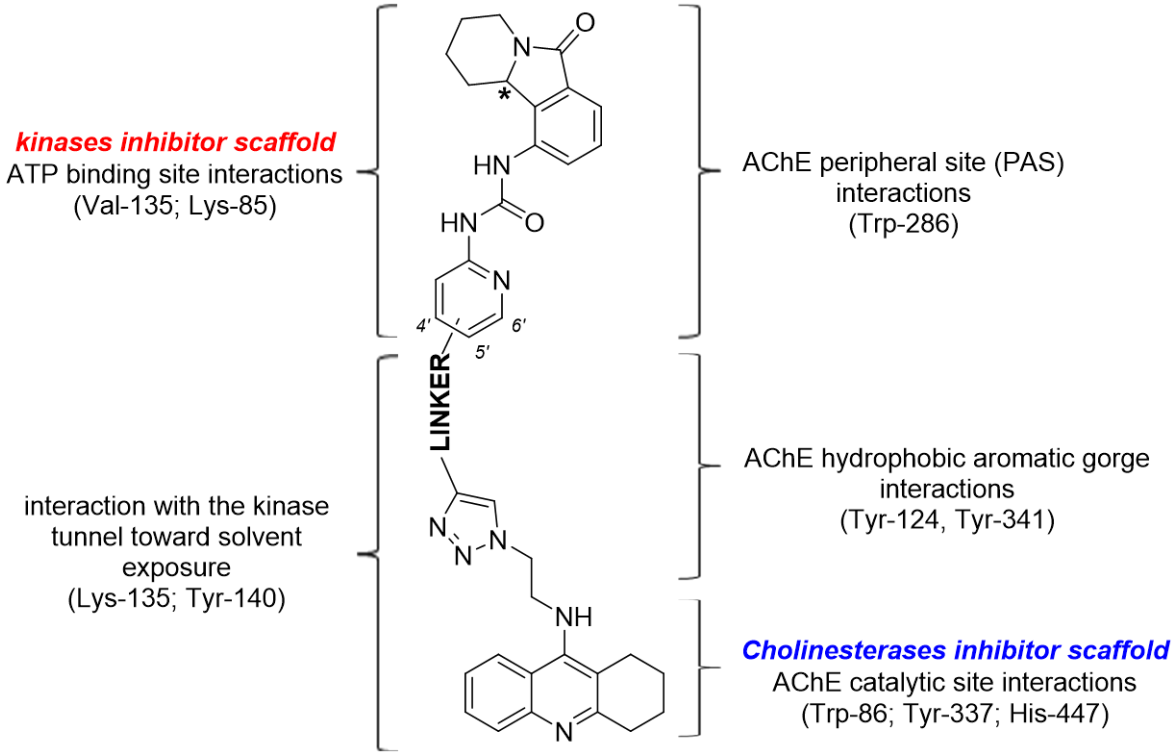

Figure 2. Design strategy of proposed MTDLs targeting both ChEs and GSK-3 kinases.

2. Results and discussion

2.1 Design and docking studies

Before investing synthetic efforts in the preparation of a large number of MTDLs, we performed modelling studies to determine the optimal length and chemical characteristics of the linker connecting the two pharmacophores. These modelling studies took as a starting point the crystal structure of the *anti*-TZ2-PA6 complex with mouse AChE (mAChE) that was referred to above (PDB 1Q84) [50]. The active-site gorge of AChE is known to display some conformational flexibility. Binding of bifunctional ligands can induce some side-chain rotations, *e.g.*, of Trp286, and movement of the protein backbone at the PAS and within the region of the gorge between the PAS and the catalytic site.[50, 53-55] Taking into account this flexibility, we modelled eight MTDLs containing different linkers between the triazole and the valmerin pyridine ring by varying the length (0-3 methylene units) and the chemical nature of the linker (a simple alkyl chain or a chain containing an oxygen atom or a tertiary amine). The docking studies were performed with both enantiomers of the tetrahydropyridoisoindolone moiety, and the linker was attached to the pyridine C-4' atom since it had been earlier reported that this position allows substitution without altering the binding activity for the targeted kinases.[56] The binding energies for AChE of these MTDLs, as calculated by use of Autodock Vina,[57] are listed in Table 1. Low binding energies, below -15.0 kcal/mol, were obtained for both enantiomers of all the tested compounds, except for the S enantiomer of **1**, which displayed a higher value, -12.8 kcal/mol. All docking poses showed a productive conformation of the tetrahydroacridine scaffold within the active site of AChE (Figure 3), with an optimal double π-π stacking interaction with Trp-86 and Tyr-337, and formation of a hydrogen bond with the backbone carbonyl group of His447. Furthermore, it superimposed very well with that of anti-TZ2-PA6 (see additional docking poses in supporting information). Moreover, the lower binding

energy predicted for **2**, relative to **3**, could be explained by an additional π-π stacking interaction observed between Trp286 and the valmerin pyridine ring.

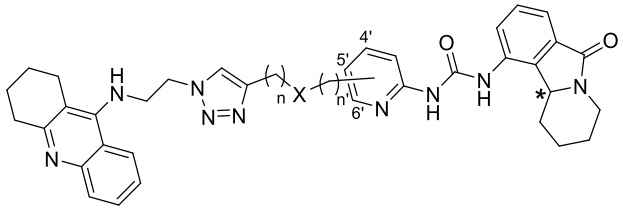

Table 1. Stabilization energies calculated for MTDLs **1-8**.

Entry	Compound	Linker position on pyridine	X	n	n'	Binding energy (kcal/mol)	
						R enantiomer	*S* enantiomer
1	**1**	4'	CH_2	1	1	-14.9	-12.8
2	**2**	4'	O	1	1	-15.2	-15.2
3	**3**	4'	N-Me	1	1	-14.3	-14.7
4	**4**	4'	CH_2	1	0	-14.6	-14.9
5	**5**	4'	CH_2	0	0	-15.8	-15.6
6	**6**	4'	Ø	0	0	-16.6	-16.8
7	**7**	5'	Ø	0	0	-16.0	-16.2
8	**8**	6'	Ø	0	0	-16.3	-16.6
9	*anti*-TZ2-PA6		-	-	-	-14.6	

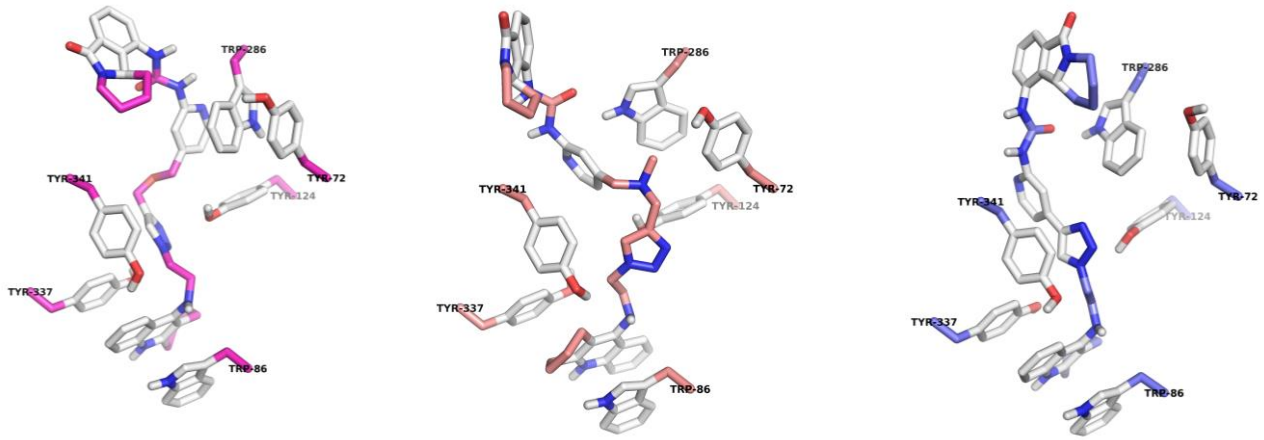

Figure 3. Molecular docking of (*R*)-**2** (left panel), (*R*)-**3** (middle panel) and (*R*)-**6** (right panel) into hAChE.

In addition, as reported for the crystal structure of the *anti*-TZ2PA6/mouse AChE complex, molecular dockings show potential hydrogen bonds between the 1,2,3-triazole moiety and Tyr124 and Tyr337. The lowest stabilization energies were obtained for the two enantiomers of **6**. This could be explained by an additional π-π stacking interaction of the triazole with Tyr341. These low stabilization energies could also be explained by hydrogen bonds formed between the C=O of the urea moiety of the valmerins and Tyr286, and between the backbone carbonyl group of Tyr341 and the NH of the urea. In addition, we modelled MTDLs **7** and **8** substituted respectively at positions C5' and C6' on the pyridine ring of the valmerins. This docking study also showed promising binding affinity toward AChE.

As a further step, MTLDs **1-8** were also docked into the crystal structure of GSK-3β (PDB code 5K5N).[58] The lowest binding energy, -10.6 kcal/mol, was obtained for the *S* enantiomer of **6** (Figure 4). In the docked structure, the tetrahydropyridoisoindole scaffold points toward the hinge region, forming a hydrogen bond between Val135 and the C=O of the isoindolone.[56] In addition, a hydrogen bond between Lys183 and triazole *N*-3 and a cation-π interaction between Lys183 and the pyridine ring were observed. As reported in our previous SAR studies,[48, 56, 59] better binding was predicted for compounds whose linker is attached to C4' of the pyridine ring. Indeed, docking poses showed that the tacrine scaffold is oriented towards the solvent, thus minimizing interaction with the kinase. Moreover, the principal docking pose seen for **6** revealed a T-shaped interaction between the tacrine scaffold and Tyr140.

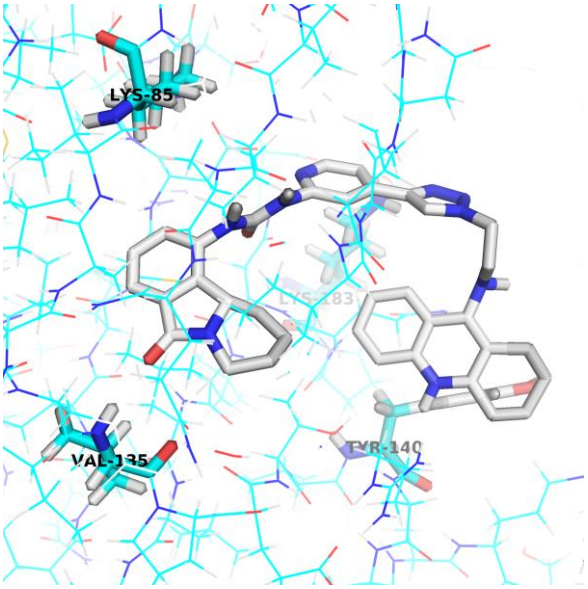

Figure 4. Docking of (*S*)-**6** into GSK-3*β*.

To validate these molecular modelling studies, we decided to synthesize the MTDLs **2**, **3**, **4, 5, 6, 7** and **8** as racemic mixtures, as well as both enantiomers of **6**, in order to determine experimentally their inhibitory activities on ChEs and selected kinases. The docking on the compound **1** presenting higher binding energies (especially for S enantiomer), we focused the synthetic efforts on the molecules presenting a binding energy lower than -14 kcal/mol for both enantiomers.

2.2 Chemistry

First, the tetrahydroacridine scaffold **14,** bearing a clickable azide moiety, was prepared from the commercially available 2-aminobenzoic acid **9** and cyclohexanone **10** (Scheme 1). The compound **14** was thus obtained in four steps with an overall yield of 18%. The detailed procedures of the synthesis of **14** are descried in supporting information.

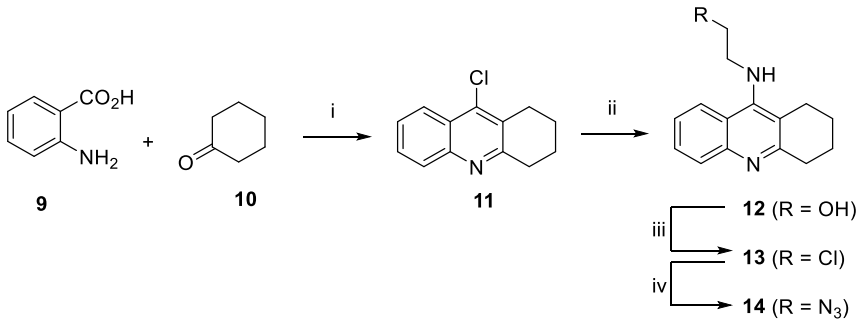

Scheme 1. Reagents and conditions. (i) $POCl_3$ (10.0 equiv), 0 °C, then 12 h reflux, 52%; (ii) ethanolamine (3.0 equiv), 18 h reflux, 76%; (iii) $SOCl_2$ (21.0 equiv), 45 min reflux, 75%; (iv) NaN_3 (4 equiv), DMF, 80 °C, 24 h, 61%.

The synthesis of the pyridine moieties **19** and **23** (Scheme 2) started with the esterification of the commercially available 4-(hydroxymethyl)picolinic acid **15** to give the corresponding methyl ester **16** in 89% yield. Then, the preparation of compound **17** consisted in a treatment of **16** with sodium hydride at 0 °C in DMF followed by the addition of propargyl bromide giving **17** in 72% yield. Treatment with an excess of hydrazine in methanol gave the acyl hydrazine **18** in a near quantitative yield. Finally, the acyl azide **19** was synthesized using sodium nitrite in aqueous 12 N HCl solution at 0 °C in 88% yield. In conclusion, acyl azide **19** was obtained in four steps from 4-(hydroxymethyl)picolinic acid **15** in a 55% overall yield.

Regarding the preparation of compound **23**, the first step consisted in the conversion of alcohol **16** to the corresponding chloride **20,** followed by the nucleophilic substitution with *N*-methylpropargyl amine in the presence of potassium carbonate in refluxing acetonitrile to give compound **21** in 74% yield. The following step consisted in the conversion of methyl ester **21** to the corresponding acyl azide **23**. In conclusion, derivative **23** was obtained in five steps from 4-(hydroxymethyl)picolinic acid **15** and in a 50% overall yield.

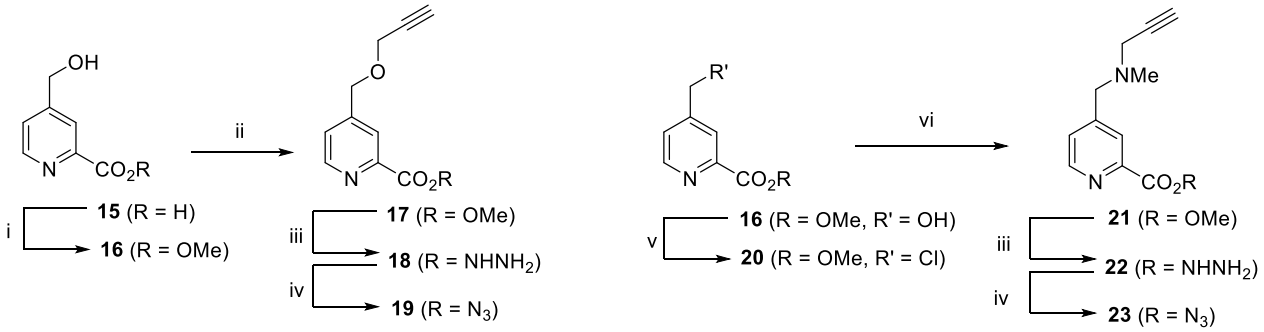

Scheme 2. Reagents and conditions. (i) $SOCl_2$ (4.0 equiv), MeOH, reflux, 48 h, 89%; (ii) NaH (2.0 equiv), propargyl bromide (80% in toluene) (2.0 equiv), DMF, 0 °C to rt, 18 h, 72%; (iii) hydrazine monohydrate (7.0 equiv), MeOH, 45 min rt, 99% for **18** and **22**; (iv) $NaNO_2$ (2.0 equiv), 12 N aqueous HCl, 0 °C, 2 h, 88% (for **19**) and 83% (for **23**); (v) Mesyl chloride (1.5 equiv), Et_3N (2.0 equiv), CH_2Cl_2, 0 °C, then 24 h reflux, 92%; (vi) *N*-methylpropargylamine (1.5 equiv), K_2CO_3 (2.0 equiv), CH_3CN, 24 h reflux, 74%.

Curtius rearrangement between acyl azides **19** and **23** with tetrahydropyrido[2,1-*a*]isoindolone (±)-**24** [60] in refluxing 1,4-dioxane led to the desired ureas (±)-**25** and (±)-**26** in 74% and 91% yield, respectively. Finally, CuAAC reaction with **14** using copper sulfate (0.3 equiv) and sodium ascorbate (0.6 equiv) in DMF for 48 h produced (±)-**2** and (±)-**3** in 65% and 72% yield, respectively (Scheme 3).

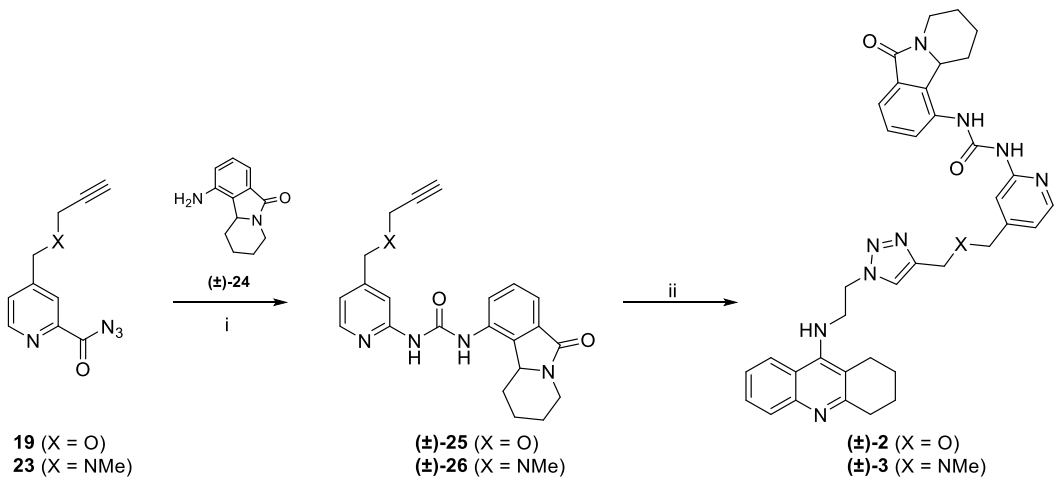

Scheme 3. Reagents and conditions. (i) (±)-**24** (1.0 equiv), 1,4-dioxane, reflux, 24 h, 74% (for (±)-**25**) and 91% (for (±)-**26**); (ii) **14** (1 equiv), $CuSO_4.5H_2O$ (0.3 equiv), sodium ascorbate (0.6 equiv), DMF, 48 h rt, 65% (for (±)-**2**), 72% (for (±)-**3**).

We subsequently decided to synthesize several fragments of **2** in order to determine their structural contributions (especially those of the tacrine and triazole scaffolds) to the inhibition of the kinases (Figure 5). Thus, **27**, **28A-C** and **29** were also prepared as described below.

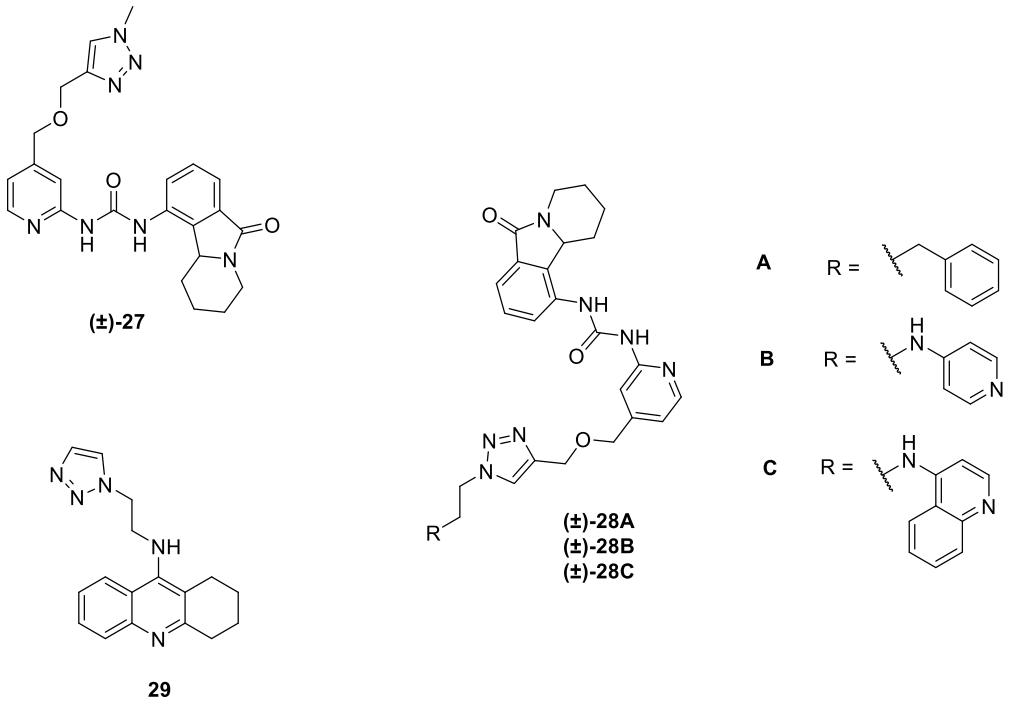

Figure 5. Structures of isoindolone and tacrine-based fragments of **2** that were synthesized.

The first step in the synthesis of (±)-**27** involved the CuAAC reaction between trimethylsilylmethyl azide and compound **17** to furnish **30** in 74% yield (Scheme 4). Treatment with TBAF yielded the *N*-methyl triazole **31** in 76% yield. The following step was formation of the acyl azide **33** from the methyl ester **31** *via* a similar route to that previously described for **2**, giving **33** in 24% overall yield. Then, Curtius rearrangement between **33** and tetrahydropyrido[2,1-*a*]isoindolone, (±)-**24**, resulted in the desired product (±)-**27**. Thus, (±)-**27** was synthesized in five steps from **17** in 3% overall yield.

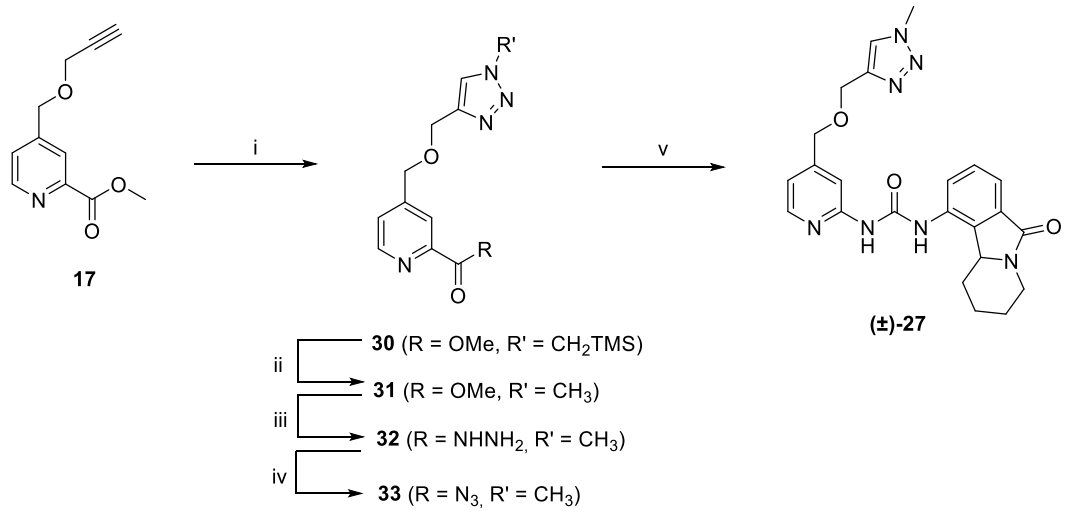

Scheme 4. Reagents and conditions. (i) trimethylsilylmethyl azide (1.1 equiv), $CuSO_4.5H_2O$ (0.3 equiv), sodium ascorbate (0.6 equiv), DMF, 24 h, rt, 74%; (ii) TBAF (1.0 M in THF) (2.0 equiv), THF, 0 °C, then 24 h rt, 76%; (iii) hydrazine monohydrate (7.0 equiv), MeOH, 45 min, rt, 99%; (iv) $NaNO_2$ (2.0 equiv), 12 N aqueous HCl, 2 h, 0 °C, 25%; (v) (±)-**24** (1.0 equiv), 1,4-dioxane, 24 h, reflux, 25%.

The syntheses of isoindolone-based fragments **28A-C** involved the CuAAC between alkyne (±)-**25** and azides **34A**,[61] **34B** and **34C**. The latter were prepared from 3-phenylpropan-1-ol, 4-aminopyridine and 4,7-dichloroquinoline, respectively (see supporting information). Using 0.3 equiv of $CuSO_4$ and 0.6 equiv of sodium ascorbate, **28A-C** were obtained in 99, 41 and 47% yields, respectively (Scheme 5).

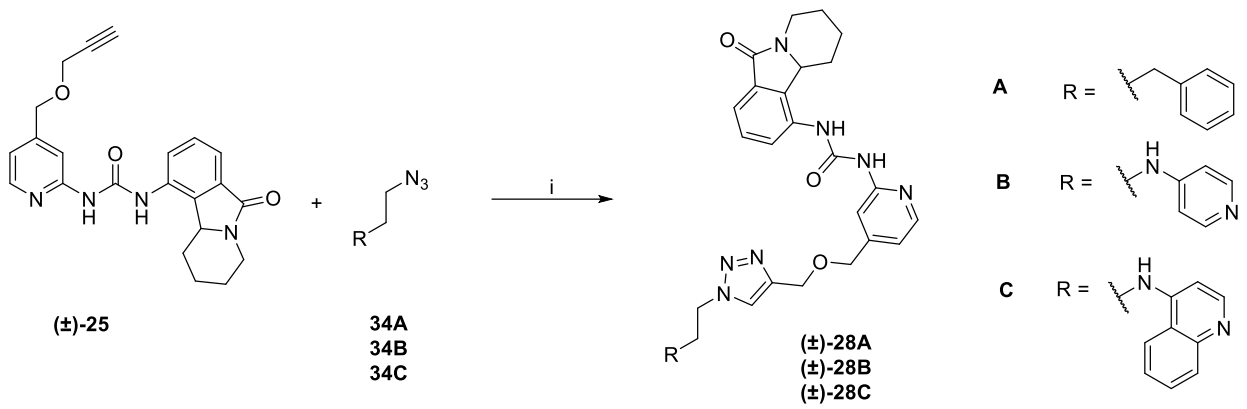

Scheme 5. Reagents and conditions. (i) **34A-C** (1.0 equiv), $CuSO_4.5H_2O$ (0.3 equiv), sodium ascorbate (0.6 equiv), DMF, 48 h, rt, 99% (for (±)-**28A**), 41% (for (±)-**28B**), 47% (for (±)-**28C**).

Finally, the tacrine-based fragment **29** was synthesized from **14** as shown in Scheme 6. The CuAAC reaction between **14** and trimethylsilylacetylene, followed by treatment with tetra-*n*-butylammonium fluoride, gave **29** in two steps in 50% overall yield.

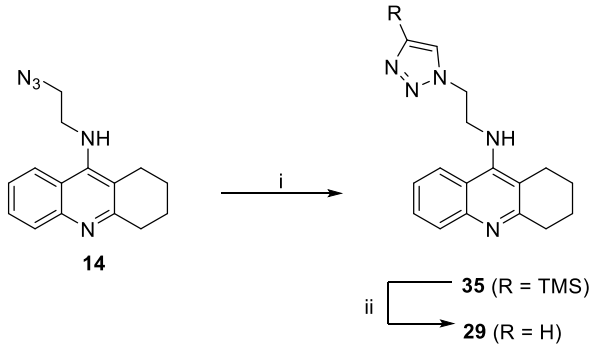

Scheme 6. Reagents and conditions. (i) trimethylsilylacetylene (1.5 equiv), $CuSO_4.5H_2O$ (0.3 equiv), sodium ascorbate (0.6 equiv), DMF, 3 h, rt, 99%; (ii) TBAF (1.0 M in THF) (2.0 equiv), THF, 3 h, reflux, 50%.

We then prepared the precursor alkynes (±)-**47** and (±)-**48** for synthesis of the MTDLs (±)-**4** and (±)-**6**, respectively (Scheme 7). Oxidation of the primary alcohols **16** and **37** to the

corresponding aldehydes **38** and **40** was performed using 2-iodoxybenzoic acid (IBX) in refluxed EtOAc in a near quantitative yield. Unfortunately, all attempts to prepare aldehyde **39** by oxidation of alcohol **36** failed. Oxidation using IBX, Dess-Martin periodinane, PCC or Swern conditions led only to degradation, probably due to the low stability of **39**, therefore we were unable to synthesis the bifunctional ligand **5**. Alcohols **36** and **37** were prepared in five steps from commercially available 4-pyridineethanol and 4-pyridinepropanol, respectively (see supporting information). Then, Seyferth-Gilbert homologation was carried out using 1.5 equivalent of the Ohira-Bestmann reagent to give the desired alkynes **41** and **42** in 36% and 48% yield respectively. Conversion of **41** and **42** to the corresponding acyl azides **45** and **46** was performed in two steps in 63% and 82% yields, respectively, as described earlier for **19** and **21**. Finally, Curtius rearrangement between acyl azides **45** and **46** and (±)-**24** gave (±)-**47** and (±)-**48** in 92% yield and 40% yield respectively.

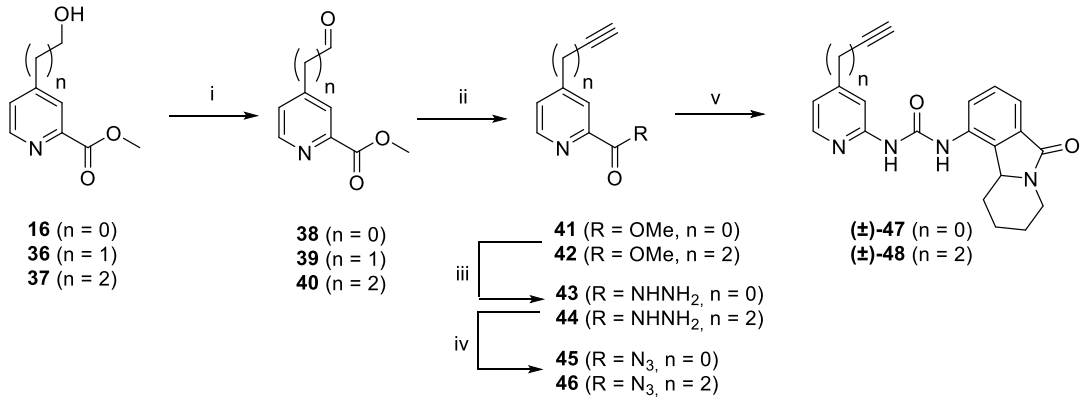

Scheme 7. Reagents and conditions. (i) IBX (3.0 equiv), EtOAc, 3 h reflux for **38**, and 12 h for **40**, 99%; (ii) Ohira-Bestmann reagent (1.5 equiv), K_2CO_3 (2.0 equiv), MeOH, rt, 36% (for **41**), 48% (for **42**); (iii) hydrazine monohydrate (7.0 equiv), MeOH, 45 min, rt, 99%; (iv) $NaNO_2$ (2.0 equiv), 12 N aqueous HCl, 2 h, 0 °C, 64% (for **45**), 83% (for **46**); (v) (±)-**24** (1.0 equiv), 1,4-dioxane, 24 h, reflux, 92% (for (±)-**47**), 40% (for (±)-**48**).

The final step in accessing the MTDLs (±)-**4** and (±)-**6** consisted of a CuAAC reaction between azide **14** and alkynes (±)-**47** and (±)-**48** (Scheme 8). Following this procedure, (±)-**4** and (±)-**6** were obtained in 19% and 18% yields, respectively.

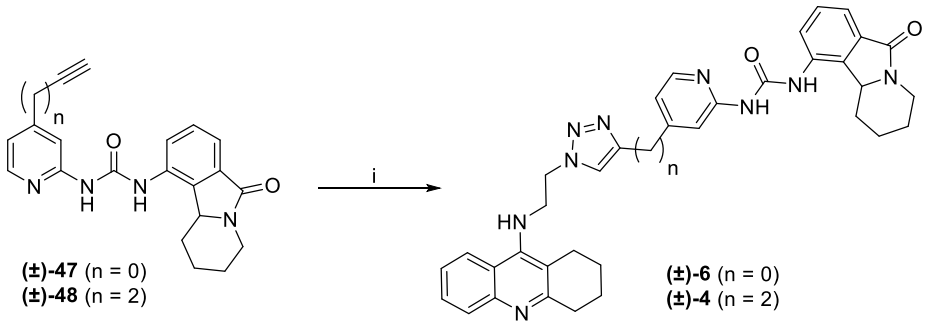

Scheme 8. Reagents and conditions. (i) **14** (1.0 equiv), $CuSO_4.5H_2O$ (0.3 equiv), sodium ascorbate (0.6 equiv), DMF, 48 h, rt, 18% for (±)-**6,** and 19% for (±)-**4**.

The syntheses of single enantiomers of **6** started with the enantioseparation of both enantiomers of (±)-**24** by supercritical fluid chromatography (SFC) (scheme 9) (see supporting information). The absolute stereochemistry of (*R*)-**24** was determined by single crystal X-ray diffraction after crystallization by vapor diffusion (CH_2Cl_2/pentane) (See supporting information). Then, Curtius rearrangement between each enantiomer of **24** and acyl azide **45** gave the corresponding optically pure ureas (*R*)-**47** and (*S*)-**47** in 73% and 76% yield, respectively. The final step consisted of a CuAAC reaction between azide **14** and alkyne (*R*)-**47** and (*S*)-**47** to furnish (*R*)-**6** and (*S*)-**6** in 56% and 45% yield, respectively. The higher yields in the CuAAC reaction achieved in the synthesis of the pure enantiomers with respect to the racemic mixtures suggests that the poor yields obtained for synthesis of (±)-**4** and (±)-**6** could be improved.

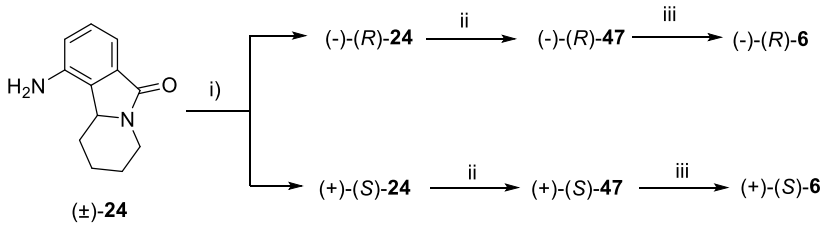

Scheme 9. Reagents and conditions. (i) Separation of enantiomers by SFC; (ii) **45** (1.0 equiv), 1,4-dioxane, 24 h reflux, 73% for (-)-(*R*)-**47**, 76% for (+)-(*S*)-**47**; (iii) **14** (1.0 equiv), $CuSO_4.5H_2O$ (0.3 equiv), sodium ascorbate (0.6 equiv), DMF, 48 h, rt, 56% for (-)-(*R*)-**6**, 45% for (+)-(*S*)-**6**.

Subsequently, we prepared both regioisomers of MTDL **6** substituted at position C-5' (Schemes 10 and 11). The syntheses started with a Sonogashira cross-coupling reaction between the commercially available bromomethyl picolinates **49** and **50** and ethynyltrimethylsilane, to furnish alkynes **51** and **52** in 97% and 96% yield, respectively. Deprotection of the alkynes was performed with potassium fluoride to give compounds **53** and **54** in 77% and 82% yield, respectively. The conversion of esters **53** and **54** to the corresponding acyl azides, **57** and **58**, was performed as previously described, in two steps, in 95% and 90% overall yields, respectively. Finally, Curtius rearrangement between acyl azides **57** and **58** and (±)-**24** gave (±)-**59** and (±)-**60** in 65% and 50% yield, respectively. To summarize, ureas (±)-**59** and (±)-**60** were prepared in five steps from methyl picolinates **49** and **50** in 46% and 35% overall yield, respectively. The last step consisted of the CuAAC reaction between azide **14** and alkynes (±)-**59** and (±)-**60** to give the MTDLs (±)-**7** and (±)-**8** in 81% and 94% yield, respectively (Scheme 11).

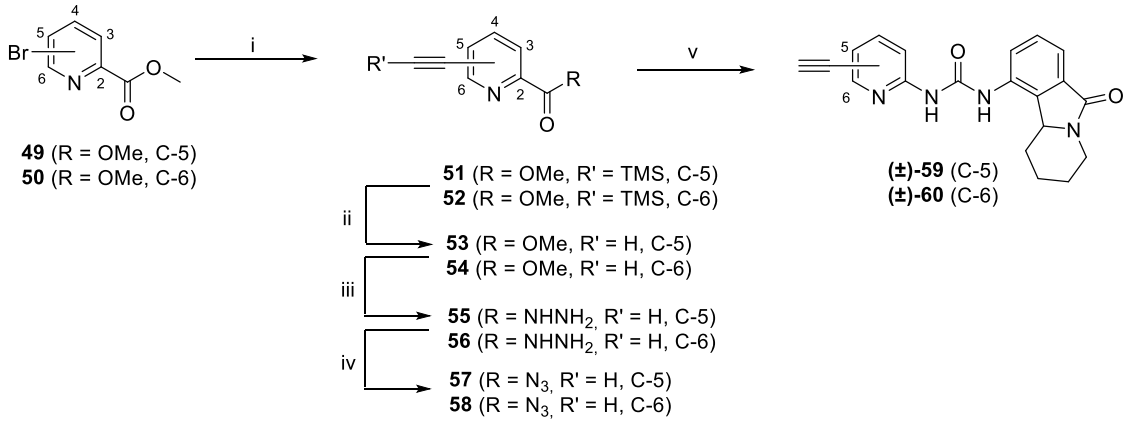

Scheme 10. Reagents and conditions. (i) Ethynyltrimethylsilane (3.0 equiv), CuI (0.1 equiv), $PdCl_2(PPh_3)_2$ (0.05 equiv), Et_3N/THF (1:1, v/v), 5 h, 60 °C, 97% for **51**, 96% for **52**; (ii) KF (3.0 equiv), MeOH/CH_2Cl_2 (1:1, v/v), 12 h, rt, 77% for **53**, 82% for **54**; (iii) hydrazine monohydrate (7.0 equiv), MeOH, 45 min, rt, 99%; (iv) $NaNO_2$ (2.0 equiv), 12 N aqueous HCl, 2 h 0 °C, 96% for **57**, 91% for **58**; (v) (±)-**24** (1.0 equiv), 1,4-dioxane, reflux for 24 h, 65% for (±)-**59**, 50% for (±)-**60**.

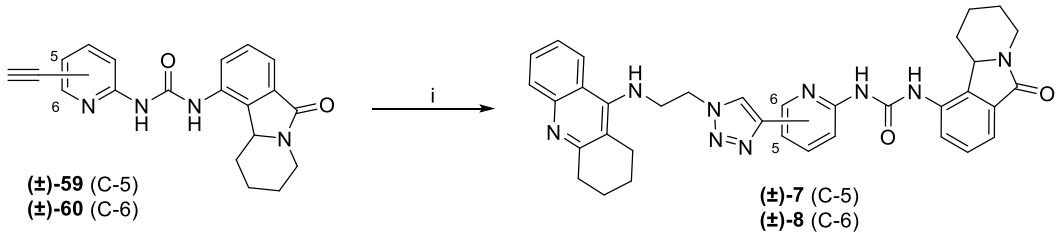

Scheme 11. (i) **14** (1.0 equiv), $CuSO_4.5H_2O$ (0.3 equiv), sodium ascorbate (0.6 equiv), DMF, 48 h rt, 81% for (±)-**7**. 94% for (±)-**8**.

2.3 *In vitro* Assays

The newly synthesized MTDLs (**±)-2-4,** (**±)-6-8**, (*R*)-**6** and *(S)*-**6,** were evaluated for their inhibitory potency on kinases GSK-3α/β and CKD5/p25, and on human AChE (hAChE) and human BChE (hBChE) (Table 2).

Table 2. Inhibition of ChEs and kinases by MTDLs (±)-**2**-**4**, (±)-**6**-**8**, (*R*)-**6** and (*S*)-**6**.

Entry	Compound	hAChE (nM)[a]	hBChE (nM)[a]	SI[b]	GSK-3α/β (nM)[c]	CDK5/p25 (nM)[c]
1	**(±)-2**	20.8 ± 0.9	169 ± 6	8.1	10	300
2	**(±)-3**	58.6 ± 3.1	206 ± 7	3.5	10	310
3	**(±)-4**	23.6 ± 2.3	65.7 ± 3.5	2.8	21	800
4	**(±)-6**	11.4 ± 1.7	301 ± 14	26	16	800
5	***(R)*-6**	9.5 ± 0.4	395 ± 27	41.5	7	500
6	***(S)*-6**	13.7 ± 1.0	254 ± 18	18.5	19	1100
7	**(±)-7**	0.8 ± 0.1	185 ± 47	227	>10000	>10000
8	**(±)-8**	133±6	21.1 ± 1.6	0.16	4200	3100

[a] Human recombinant AChE and BChE from human serum were used. Values are expressed as the mean ± SEM of two independent experiments each performed in triplicate. [b] Selectivity Index SI: IC_{50} (hBChE)/IC_{50} (hAChE). [c]All data points for construction of dose-response curves were recorded in triplicate. Typically, the standard deviation of single data points was below 10%.

In addition, the inhibitory activity, expressed as IC_{50} values, toward GSK-3α/β and CKD5/p25 of all isoindolone-based fragments, i.e., (±)-**25**-**27**, (**±**)-**28A**-**C**, (**±**)-**47**, (***R*)-47**, (***S*)-47**, (**±**)-**48**, (**±**)-**59** and (**±**)-**60** and of the tacrine-based fragment **29** were determined and are listed in Table 3.

Table 3. Kinase inhibition by isoindolone-based and tacrine-based fragments.

		IC_{50} (nM)[a]	
Entry	Compound	GSK-3α/β	CDK5/p25
1	**(±)-25**	60	150
2	**(±)-26**	11	90
3	**(±)-27**	25	250
4	**(±)-28A**	8	260
5	**(±)-28B**	30	200
6	**(±)-28C**	>10 000	240
7	**29**	>10 000	>10 000
8	**(±)-47**	41	68
9	***(R)*-47**	33	18
10	***(S)*-47**	90	50
11	**(±)-48**	15	70
12	**(±)-59**	>10 000	>10 000
13	**(±)-60**	300	80

[a]All data points for construction of dose-response curves were recorded in triplicate. Typically, the standard deviation of single data points was below 10%.

The most active inhibitor (±)-**7** showed a very high inhibitory potency in the subnanomolar range (IC_{50} = 815 pM). However, all the other assayed hybrids were active against hAChE in the nanomolar concentration range (Table 2). In detail, the hybrid (±)-**2** was 2.8-fold more potent

than compound (±)-**3** probably due a better interaction of the pyridine ring with Trp-286 at the PAS of AChE. In addition, as predicted by docking studies, the shorter the linker between triazole and pyridine ring is, the better the inhibitory potency. For instance, compound (±)-**6** was 2-fold more potent than compound (±)-**4**, 1.8-fold more potent than compound (±)-**2** and 5-fold more potent than compound (±)-**3**. Regarding the enantiomers of hybrid **6**, the enantiomer (*R*)-**6** was only 1.5-fold more potent than the enantiomer (*S*)-**6**. All MTDLs, except (±)-**8**, showed selectivity of one order of magnitude toward hAChE as compared with hBChE, except for compound (±)-**7**, which was 227-fold more potent on hAChE. Conversely (±)-**8** acted as a BChE selective inhibitor. Among all the hybrids, compound (±)-**8** showed the highest potency and selectivity toward hBChE with an IC_{50} value of 21.1 nM and a selectivity index vs hAChE of 6.3. As well reported, BChE inhibition could be also benefit for AD patients.[62]

Interestingly, compounds (±)-**2**, (±)-**3**, (±)-**4** and (±)-**6** showed an inhibitory activity in the nanomolar range toward GSK-3 α/β (Table 2). As reported in previous studies, the substitution of the linker on the pyridine position C-4' proved to be the most suitable to preserve a strong inhibitory activity toward GSK-3 α/β. In detail, compound (±)-**6** was 625-fold and 262-fold more potent than compounds (±)-**7** and (±)-**8**, whose linker is attached on positions C-5' and 6' on the pyridine, respectively. Conversely to the parent valmerins (Figure 1), all new hybrids showed low inhibitory potency toward CDK5 kinases, and thus a selectivity for GSK-3 α/β (table 2). As far as the influence of the absolute configuration of the stereocentre of the isoindolone scaffold is concerned, (*R*)-**6** exhibited a GSK-3 kinase inhibition potency around three times higher than the (*S*)-enantiomer. This relatively small difference indicates that the shape differences of the isoindolone scaffold related to its stereocentre absolute configuration are limited.

The determination of the inhibitory activity of the isoindolone-based and tacrine-based fragments (Table 3) provided additional information for the definition of the SAR study, especially regarding the contribution of the tacrine and triazole moieties to kinase inhibition. Indeed, the racemic hybrid (±)-**2** was 6-fold more potent than its precursor (±)-**25**, indicating that the triazole or/and tacrine scaffolds contributed to the kinase inhibition. This difference of potency was not observed for compound (±)-**3** and its precursor (±)-**26** probably due to an additional interaction of the *N*-Me group within the GSK-3 active site. Addition of the triazole ring allowed a good GSK-3 binding mode. For instance, hybrid (±)-**27** containing a triazole ring was 2.4-fold greater inhibitor than (±)-**25**. In contrast, depletion of the isoindolone scaffold, such as in compound **29** led to a complete loss of activity toward GSK-3 (IC_{50} > 10 μM). These results suggested a synergistic effect of the triazole and isoindolone scaffolds in GSK-3 inhibition. The addition of a hydrophobic moiety led to an increase in the inhibitory potency of the isoindolone. In comparison with compound (±)-**27**, the isoindolone-based fragment (±)-**28A** was a 3-fold more potent GSK-3 inhibitor. In contrast, the addition of more polar substituents (e.g., 4-aminopyridine and 4-aminoquinoline) decreased the binding affinity toward GSK-3 kinase (up to 1250-fold less potent). I*n vitro* results confirmed the importance of the triazole in kinase inhibition. Indeed, (*S*)-**6** and (*R*)-**6** were up to 4.7-fold more potent than their precursor (*S*)-**47** and (*R*)-**47** respectively. Finally, as reported in previous results, the substitution in position 5 or 6 on the pyridine ring had a deleterious effect for the inhibition of GSK-3 kinase. Only the isoindolone-based fragment (*R*)-**47** showed inhibition potency toward CDK5 in the nanomolar range (IC_{50} = 18 nM). In conclusion, the hybrid (*R*)-**6** showed the most promising MTDL profile for the inhibition of hAChE and GSK-3α/β with potencies in the nanomolar range for both enzymes (e.g., IC_{50} = 9.5 nM for hAChE and 7 nM for GSK-3 α/β). These results also

highlighted the synergistic effect of the triazole and isoindolone scaffolds in the inhibition of GSK-3α/β.

The selectivity of (±)-**6** (10 μM) was also evaluated on a panel of 468 kinases (Discoverx, Kinomescan^{TM}). The results showed that (±)-**6** displayed a poor selectivity and several kinases are targeted (see supporting information). At this concentration (10 μM), (±)-**6** displayed a weak inhibition of GSK-3β (17%) whereas a total inhibition of GSK-3α was observed.

2.4 Cell-based assays: Cytotoxicity and Brain Penetration

The cytotoxicity of these new MTDL hybrids were evaluated against a panel of representative human cell lines including HuH7 (liver), Caco2 (colon), MDA-MB231 (breast), HCT-116 (colon), PC3 (prostate), NCIH727 (lung), HaCaT (skin). The concentrations responsible for 50% inhibition of cell growth are reported in table 4. Interestingly, the new hybrids were significantly less cytotoxic whereas the tacrine fragment exhibited IC_{50} values in the micromolar range and the isoindolone fragments in the nanomolar range, thus proving to be quite toxic. In general, **(±)-2-4**, **(±)-6-8,** (*R*)-**6** and *(S)*-**6** were scarcely cytotoxic with IC_{50} values in the micromolar range regardless the cell line. Hybrids **(±)-7** and **(±)-8** presented the lowest cytotoxicity with a double-digit micromolar IC_{50} range (higher than 25 μM for **(±)-7**), while compound **(±)-4** showed a slightly higher cytotoxicity with IC_{50} values of 1.1 ± 0.4 μM for colon HCT 116 cell lines.

Table 4: Cytotoxicity of MTDLs on human cell lines

		IC_{50} (μM) on Human cell lines[a]							
Entry	MTDL	HuH7	Caco2	MDA-MB231	HCT-116	PC3	NCI-H727	HaCaT	Fibroblast
1	**(±)-2**	4.0 ± 0.4	20 ± 3	4.0 ± 0.4	4.0 ± 0.4	7.0 ± 0.1	9 ± 2	4.0 ± 0.4	3 ± 0.5
2	**(±)-3**	2.0 ± 0.3	9.0 ± 0.3	2.0 ± 0.1	2.0 ± 0.1	3.0 ± 0.3	4.0 ± 0.6	2.0 ± 0.1	2 ± 0.2
3	**(±)-4**	2.9 ± 0.4	4.8 ± 0.6	2.0 ± 0.1	1.1 ± 0.4	1.6 ± 0.1	6.3 ± 1.5	1.9 ± 0.2	4.0 ± 0.6
4	**(±)-6**	3.0 ± 0.9	3.0 ± 0.6	2.0 ± 0.1	3.0 ± 0.5	5 ± 1	2.0 ± 0.3	5.0 ± 0.2	>25
5	***(R)*-6**	3.5 ± 0.3	8 ± 1	2.0 ± 0.2	2.2 ± 0.1	3.0 ± 0.3	5.0 ± 0.9	-[b]	0.9 ± 0.1
6	***(S)*-6**	2.6 ± 0.5	10 ± 1	4.0 ± 0.3	2.7 ± 0.1	6.0 ± 0.9	7.0 ± 0.8	-[b]	2 ± 0.3
7	**(±)-7**	>25	>25	>25	>25	>25	>25	-[b]	0.6 ± 0.1
8	**(±)-8**	18 ± 7	24 ± 3	17 ± 1	17 ± 2	27 ± 3	>25	-[b]	17 ± 2

[a] Values are expressed as the mean of triplicate ± SD. [b] not determined.

Then, the ability of compounds **(±)-2**, **(±)-3** and **(±)-6** to interfere with the viability of neuroblastoma cells SHSY5Y after incubation for 24 h and 72 h was determined as a function of drug concentrations ranging between 0.1 and 100 μM. After 24 h, a reduction of cell viability of SHSY5Y was observed for all selected compounds; in details, at the highest tested concentration (100 μM) cell viability was decreased about 50% as compared to control (untreated) cells. After 72 h, SHSY5Y cells showed a higher sensitivity to the compounds (Figure 6) and it was possible to determine the concentrations that induced 50% of cell death (IC_{50}, μM). The IC_{50} values of compounds **(±)-2**, **(±)-3** and **(±)-6** were 22 ± 2 , 25 ± 2 and 13 ± 2 μM respectively.

In order to exclude any cytotoxic effect of the compounds on MDCK-MDR1 cells during the permeability experiments, we performed the MTT assay on MDCK-MDR1 after incubation with compounds for 2 h at 75 μM. None of the compounds affected the cell viability of MDCK-MDR1 in the conditions described above (data not shown).

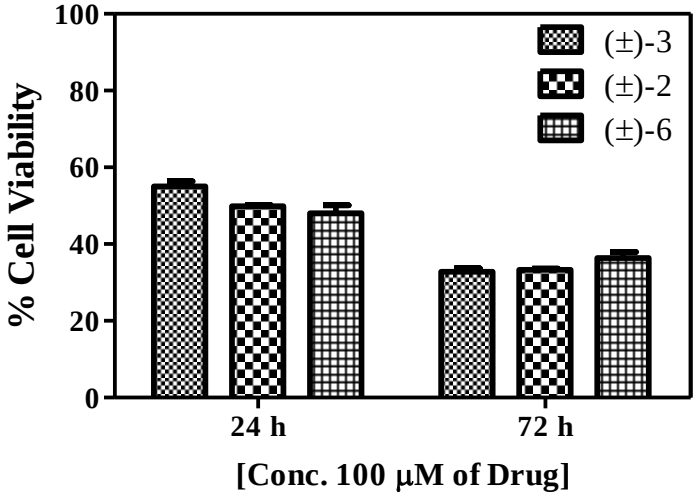

Figure 6. Percentage of cell viability of SHSY5Y neuroblastoma cells after 24 h and 72 h of co-incubation with compounds at a concentration of 100 μM.

Table 5: Bidirectional Transport across MDCKII-MDR1 Cells of Compounds **(±)-2**, **(±)-3** and **(±)-6**

Compound	$P_{app}AP$ ($\times 10^{-5}$cm/sec)	$P_{app}BL$ ($\times 10^{-5}$cm/sec)	ER[a]
(±)-2	1.35 ± 0.21	2.08 ± 0.18	1.54
(±)-3	1.01 ± 0.30	0.84± 0.16	0.83
(±)-6	1.11 ± 0.25	1.68 ± 0.11	1.51
Diazepam	2.02 ± 0.15	1.43 ± 0.21	0.70
FD4	0.69 ± 0.10	0.64 ± 0.16	0.93

[a] Efflux ratio (ER) was calculated using the following equation: ER = $P_{app}BL/P_{app}AP$. An efflux ratio greater than 2 indicates that the test compound is likely to be a substrate for P-gp transport.

The MDCK-MDR1 cell line expressing the P-gp represents a well-established model to mimic the BBB.[63] According to a protocol previously described,[64] we determined the Apical (AP) to Basolateral (BL) ($P_{app}AP$) and the Basolateral to Apical ($P_{app}BL$) permeabilities of sample compounds and of the markers of transcellular and paracellular pathways (Diazepam and FD4, respectively). The results reported in Table 5 showed that compounds **(±)-2**, **(±)-3** and **(±)-6** have high permeability values, comparable to that of diazepam. As they have an efflux ratio less than 2, they cannot be considered substrates for P-gp.

2.5 Crystal structures of MTDL/TcAChE complexes

To obtain structural insight into the mode of interaction of these novel MTDLs with AChE, crystal structures of the complexes of (*R*)-**2**, (*R*)-**3**, and (*S*)-**6** with *Torpedo californica* AChE (*Tc*AChE) were obtained. The crystalline complexes were obtained by soaking the *Tc*AChE crystals for 12 h in mother liquor solution containing 1 mM compound. Soaking of other MTDLs

did not yield crystals that diffracted satisfactorily. Data collection and processing, and structure refinement, are described in the experimental section and supporting information.

In the following text and in the accompanying figures, residue numbering will be that for *Tc*AChE, but for further clarity and to ensure complementarity with molecular docking section, *m*AChE numbering will be shown in brackets. All three inhibitors for which crystalline complexes were obtained are tacrine-based, and the tacrine moiety bound as previously observed for tacrine itself. Thus, in all three crystal structures, the tacrine moiety is stacked between Trp84 (Trp86) and Phe330 (Tyr337) (Figure 7). It is also H-bonded to the carbonyl of His440 (His447), and fits into the hydrophobic groove of the active-site, which is composed of Trp432 (Trp439), Phe330 (Tyr337), Ile439 (Pro446), and Tyr442 (Tyr449). In all 3 complexes, the triazole ring is in the narrowest region of the gorge, interacting *via* perpendicular π-stacking interactions with Phe330 (Tyr337) and Tyr121 (Tyr124).

Here, two complex crystal structures illustrate the binding mode of compounds with an identical linker length (3 atoms), but with different chemical compositions: a single oxygen atom in **2** (PDB code 6H12) and an *N*-Me group in **3** (PDB code 6H13). These two compounds present identical binding modes, with the pyridine ring of the valmerin engaged in a π-stacking interaction with Trp279 (Trp286) of the PAS (Figures 7A and 7B). However, there is a 2-fold difference in the inhibition potency of these compounds, with **2** binding more strongly (Table 2). The Protein-Ligand Interaction Profiler (plip) server,[65] which identifies non-covalent interactions between ligands and proteins, has been used to finely compare the binding modes of **2** and **3**. Two perpendicular π-stacking interactions were observed between **2** and Trp 279 (Trp 286)**,** but only one is present for **3**. The linker of **2**, which contains an oxygen atom, seems to afford more flexibility, thus permitting enhanced interaction between the pyridine ring of the

valmerin and Trp279 (Trp286). This is the only structural difference that could be accounted for in the crystal srtuctures of *Tc*AChE in complex with **2** and **3**, and thus could be considered responsible for the higher affinity of **2** for AChE In neither of these two crystal structures any interaction is observed between the protein and the tetrahydropyridoisoindolone core of the valmerin.

The third crystal structure presented here is the complex of **6** with *Tc*AChE (PDB code 6H14). Unlike compounds **2** and **3**, there is no linker between the two pharmacophores. While the tacrine moiety of **6** binds like tacrine itself, and the tacrine moiety in both **2** and **3**, the absence of a linker induces a slight reorientation of the triazole ring in the active-site gorge; furthermore, the side-chain of Tyr334 moves closer to the triazole ring, so that its phenolic ring is perpendicularly π-stacked against it (Figure 7C). The pyridine ring of valmerin does not interact with the PAS, but lies more deeply in the enzyme, interacting in an hydrophobic region of the gorge, more specifically with residues Phe290 (Phe297) and Phe331 (Phe338), while its nitrogen atom is H-bonded to the main-chain nitrogen of Phe288 (Phe295). The higher affinity of **6** for AChE as compared with **2** and **3** could be attibuted to these additional interactions. In this crystal structure, two conformations are observed for the tetrahydropyridoisoindolone core of the valmerin. While one of these conformations involves a symmetry-related copy of the enzyme, and is thus most probably not biologically relevant, the second conformation reveals a π-stacking interaction between the conjugated ring of the tetrahydropyridoisoindolone and Trp279 (Trp286), as well as hydrophobic interactions with both Trp279 (Trp286) and Leu282 (Leu289) (Figure 7C). The enhanced inhibitory potency of **6**, which is devoid of a linker, when compared to **2** and **3**, most probably results from a larger number of interactions between the valmerin moiety and the protein. Finally, the position of the linker on the pyridine ring seems to influence

the inhibitory capacity for AChE of these MTLDs. While for **6** substitution is at position 4, substitution at position 5 (compound **7**) and position 6 (compound **8**) increases AChE inhibition ~ 10 fold and decreases ~ 11.6 fold, respectively. Although no crystal structures could be obtained for **7** or **8**, these results suggest that the position of the linker subsitution on the pyridine ring affects the capacity of the tetrahydropyridoisoindolone moiety to interact with the PAS.

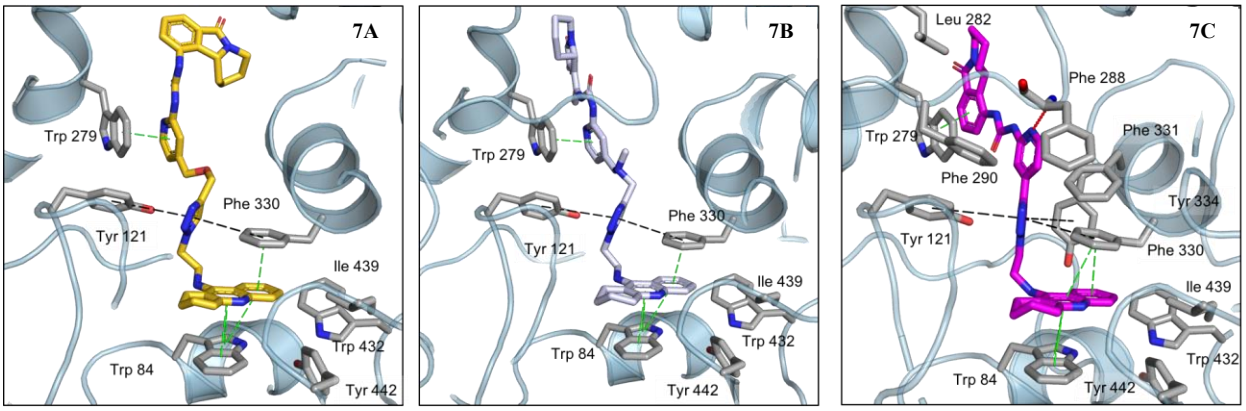

Figure 7. Crystal structures of complexes of *Tc*AChE with compound (*R*)-**2** (left-hand panel) (PDB code 6H12), compound (*R*)-**3** (central panel) (PDB code 6H13) and compound (*S*)-**6** (right-hand panel) (PDB code 6H14). The protein main chain is displayed in cartoon mode, with key residues involved in binding the ligand depicted as grey sticks. Parallel and perpendicular π-stacking interactions are shown as green and black dashed lines, respectively. A hydrogen bond in the right-hand panel is represented as red lines. If represented as sticks, an aromatic residue is in hydrophobic interaction with the compound.

3. Conclusions

Based on rational design backed with molecular docking studies performed on AChE and GSK-3β, we have synthesized a series of eight new hybrid MTDLs containing tacrine and isoindolone scaffolds by using the CuAAC reaction to link the two moieties. Amongst these novel MTDLs, compound (*R*)-**6** showed the most promising *in vitro* potencies, inhibiting both human AChE and GSK-3α/β in the same nanomolar range (9.5 and 7 nM, respectively). The crystal structures of *Tc*AChE complexed with (*R*)-**2**, (*R*)-**3** and (*S*)-**6** revealed how the linker can modify the affinity of the compound for its target, and how the plasticity of the active-site gorge permits accommodation of such MTDLs. The SAR study also revealed the anticipated importance of the triazole moiety in the inhibition of AChE, as well as its unanticipated involvement in the inhibition of GSK-3α/β. Conversely to their isoindolone- and tacrine-based fragments, all these MTDLs displayed a weak cytotoxicity toward a panel of cell lines including the liver HuH7 cell line, thus predicting low hepatotoxicity for this series of MTDLs that target two enzymes associated with AD, namely human AChE and GSK-3α/β. Moreover, bidirectional transport studies on MDCKII-MDR1 model showed a good BBB penetration of these MTDLs without interacting with the P-gp efflux system.

4. Experimental section

4.1 Chemistry

4.1.1 General

Solvents were purified by a dry solvent station MB-SPS-800 (MBraun) immediately prior to use. Triethylamine was distilled from CaH_2 and stored over BaO or KOH. All reagents were obtained from commercial suppliers (Sigma Aldrich, Acros, TCI) unless otherwise stated. Column chromatography purifications were performed on silica gel (40–63 μm) from Macherey-

Nagel. Thin-layer chromatography (TLC) was carried out on Merck DC Kieselgel 60 F-254 aluminium sheets. Compounds were visualized by UV irradiation and/or spraying with a solution of potassium permanganate, followed by charring at 150 °C. ^{1}H and ^{13}C NMR spectra were recorded with a Bruker DPX 300 spectrometer (Bruker, Wissembourg, France). Chemical shifts are expressed in parts per million (ppm) from $CDCl_3$ (δ_H = 7.26 ppm, δ_C = 77.16 ppm), and CD_3OD (δ_H = 3.31 ppm, δ_C = 49.00 ppm). J values are expressed in Hz. Mass spectra were obtained with a Finnigan LCQ Advantage MAX (ion trap) apparatus equipped with an electrospray source. High-resolution mass spectra were obtained with a Varian MAT 311 spectrometer using electrospray analysis. Analytical HPLC was performed on a Thermo Electron Surveyor instrument equipped with a PDA detector under the following conditions: Thermo Hypersil GOLD C18 column (5 µm, 4.6 x 100 mm), with 0.1% aq. TFA/ CH_3CN (90/10) as eluent (5 min), followed by a linear 10-100% CH_3CN gradient (45 min), at a flow rate of 1.0 mL/min and with *UV detection Max Plot* 220−360 nm. Optical rotations were measured at room temperature in a 10 cm cell on a Perkin–Elmer 341 LC polarimeter. Specific rotation values are given in units of 10^{-1} deg.cm^2.g^{-1}. Supercritical fluid chromatography was performed using a Waters Investigator SFC system under the following conditions: IA column (4.6 x 250 mm) with isocratic elution (ethanol/ isopropylamine, 70/30) at a flow rate of 4 mL/min, with a pressure of 120 bars, at 35 °C, monitoring at 282 nm. The synthesis of (±)-**24** was reported previously [60] and separation of the enantiomers by SFC is reported in the supporting information. The syntheses of azides **34A-C** are also reported in the supporting information.

4.1.2. General procedures A for the synthesis of acyl hydrazine.

To a stirred solution of methyl ester (1.0 equiv) in MeOH (0.3 mol/L) was added hydrazine monohydrate (7.0 equiv). After 45 min, the mixture was concentrated under reduced pressure without further purification.

4.1.3. General procedure B for the synthesis of acyl azide.

To a cooled solution of HCl 12 N (22.0 equiv) was added by portion at 0 °C acyl hydrazine (1.0 equiv). After solubilization, $NaNO_2$ (2.5 equiv) in water (0.6 g/mL) was slowly added. The mixture was stirred at 0 °C for 2 h, and quenched with a saturated aqueous solution of $NaHCO_3$, pH, 8.0. The aqueous layer was extracted three times with Et_2O. The organic phase was washed with brine, dried over $MgSO_4$, filtered, and concentrated under reduced pressure without further purification.

4.1.4. General procedure C for the synthesis of urea (Curtius rearrangement)

An acyl azide derivate (1.0 equiv) and tetrahydropyrido[2,1-*a*]isoindolone (±)-**24** (1.0 equiv) were added to dry 1,4-dioxane at final concentrations of 0.025 M. The mixture was stirred under reflux for 24 h. After cooling, the mixture was concentrated under reduced pressure, and directly purified by chromatography on silica gel.

4.1.5. General procedure D for CuAAC

A mixture of alkyne (1 equiv), azide (1.0 equiv), $CuSO_4.H_2O$ (0.3 equiv.) and sodium ascorbate (0.6 equiv) in DMF was stirred for 24 h, concentrated under reduced pressure, and purified by chromatography on silica gel.

4.1.6. Methyl 4-(hydroxymethyl)picolinate (16).

To a stirred solution of 4-(hydroxymethyl)picolinic acid **15** (4.00 g, 26.1 mmol) in MeOH (130 mL) at 0 °C was slowly added thionyl chloride (3.81mL, 52.6 mmol), followed by reflux for 24 h. After cooling to 0 °C, thionyl chloride (3.81 mL, 52.6 mmol) was again added, followed by reflux for 24 h. The mixture was then concentrated *in vacuo*, and saturated aqueous $NaHCO_3$ was added until pH 9 was reached. The aqueous layer was then extracted three times with EtOAc. The organic phase was washed with brine, dried over $MgSO_4$, filtered, and concentrated *in vacuo* without further purification to afford **16** as a white solid in 89% yield (3.90 g). ^{1}H NMR (300 MHz, $CDCl_3$) δ 8.71 (dd, J = 5.0, 0.6 Hz, 1H), 8.13 (dd, J = 1.7, 0.8 Hz, 1H), 7.51 (m, 1H), 4.84 (s, 2H), 4.01 (s, 3H). ^{13}C NMR (75 MHz, $CDCl_3$) δ 165.46, 152.82, 149.35, 147.32, 124.37, 122.55, 62.56, 52.77. MS (ESI+): *m/z* (%): 168 (100) $[M+H]^+$.

*4.1.7. Methyl 4-((prop-2-ynyloxy)methyl)picolinate (**17**).*

To a stirred solution of methyl 4-(hydroxymethyl)picolinate **16** (1.5 g, 8.9 mmol) in dry DMF (125 mL) at 0 °C was added NaH (60% dispersion in mineral oil) (718 mg, 17.9 mmol). After 1 h, propargyl bromide (80% in toluene) (1.93 mL, 17.9 mmol) was slowly added, followed by stirring for 1 h. The mixture was then stirred at room temperature for 18 h, and quenched with saturated aqueous NH_4Cl. The resulting mixture was concentrated *in vacuo* and water then

added. The aqueous layer was extracted with EtOAc (x3). The organic phase was washed with brine, dried over $MgSO_4$, filtered and concentrated *in vacuo*. The residue was purified by chromatography on silica gel (CH_2Cl_2/EtOAc 90/10, v/v) to afford **17** as a brown oil in 72% yield (1.33g). ^{1}H NMR (300 MHz, $CDCl_3$) δ 8.71 (dd, *J* = 4.9, 0.6 Hz, 1H), 8.11 (dd, *J* = 1.6, 0.8 Hz, 1H), 7.48 (dd, *J* = 4.9, 1.7 Hz, 1H), 4.69 (s, 2H), 4.27 (d, *J* = 2.4 Hz, 2H), 4.01 (s, 3H), 2.50 (t, *J* = 2.4 Hz, 1H). ^{13}C NMR (75 MHz, $CDCl_3$) δ 165.8, 150.1, 148.5, 148.2, 125.1, 123.5, 78.9, 75.6, 69.5, 58.2, 53.1. MS (ESI+): *m/z* (%): 206 (100) $[M+H]^+$.

*4.1.8. 4-((Prop-2-yn-1-yloxy)methyl)picolinohydrazide (**18**).*

General procedure A was followed using methyl ester **17** (700 mg, 3.4 mmol) to give **18** as a yellow solid (700 mg) in 99% yield. ^{1}H NMR (300 MHz, $CDCl_3$) δ 8.97 (s, 1H), 8.52 (d, *J* = 5.0 Hz, 1H), 8.11 (dd, *J* = 1.6, 0.8 Hz, 1H), 7.46 (dd, *J* = 5.0, 1.7 Hz, 1H), 4.69 (s, 2H), 4.26 (d, *J* = 2.4 Hz, 2H), 4.08 (s, 2H), 2.50 (t, *J* = 2.4 Hz, 1H). ^{13}C NMR (75 MHz, $CDCl_3$) δ 164.8, 149.3, 148.7, 148.7, 124.7, 120.6, 79.0, 75.6, 69.7, 58.2. MS (ESI+): *m/z* (%): 206 (100) $[M+H]^+$.

*4.1.9. 4-((Prop-2-yn-1-yloxy)methyl)picolinoyl azide (**19**).*

General procedure B was followed, using acyl hydrazine **18** (460 mg) to give the desired acyl azide **19** (426 mg) as a white solid in 88% yield. ^{1}H NMR (300 MHz, $CDCl_3$) δ 8.69 (d, *J* = 4.9 Hz, 1H), 8.12 (d, *J* = 0.7 Hz, 1H), 7.54 (dd, *J* = 4.9, 1.5 Hz, 1H), 4.70 (s, 2H), 4.28 (d, *J* = 2.4 Hz, 2H), 2.51 (t, *J* = 2.4 Hz, 1H). ^{13}C NMR (75 MHz, $CDCl_3$) δ 172.06, 150.08, 148.86, 148.12, 126.13, 122.94, 78.77, 75.70, 69.33, 58.29. MS (ESI+): *m/z* (%): 216 (100) $[M+H]^+$.

*4.1.10. (±)-1-(6-Oxo-1,2,3,4,6,10b-hexahydropyrido[2,1-a]isoindol-10-yl)-3-(4-((prop-2-yn-1-yloxy)methyl)pyridin-2-yl)urea (**(±)-25**).*

General procedure C was followed, using the acyl azide **19** (59 mg) and tetrahydropyrido[2,1-*a*]isoindolone **(±)-24** (50 mg). Purification by flash chromatography using (CH_2Cl_2/MeOH/NH_4OH, 98:2:1, v/v/v) gave the urea **(±)-25** (70 mg) as a beige solid in 74% yield. ^{1}H NMR (300 MHz, DMSO) δ 11.22 (s, 1H), 9.93 (s, 1H), 8.27 – 8.22 (m, 2H), 7.46 (t, *J* = 7.7 Hz, 1H), 7.39 (dd, *J* = 7.4, 1.1 Hz, 1H), 7.29 (s, 1H), 7.01 (dd, *J* = 5.3, 1.3 Hz, 1H), 4.57 (s, 2H), 4.27 (d, *J* = 2.4 Hz, 2H), 3.54 (t, *J* = 2.4 Hz, 1H), 3.05 (t, *J* = 11.4 Hz, 1H), 2.72 (dd, *J* = 7.2, 5.4 Hz, 1H), 2.29 – 2.24 (m, 1H), 1.92 (d, *J* = 13.2 Hz, 1H), 1.76 (t, *J* = 12.2 Hz, 2H), 1.34 – 1.16 (m, 1H), 0.96 – 0.81 (m, 2H). ^{13}C NMR (75 MHz, DMSO) δ 164.6, 153.1, 152.1, 150.0, 146.1, 134.8, 134.0, 132.9, 128.9, 122.2, 117.3, 115.9, 109.6, 79.8, 77.9, 69.2, 57.5, 57.3, 30.0, 25.1, 23.0. MS (ESI+): *m/z* (%): 780 (100) $[2M+H]^+$, 391 (32) $[M+H]^+$. HRMS (ESI+): *m/z* calc. for $C_{22}H_{23}N_4O_3$ 391.1692; found 391.1770. HPLC: t_R = 22.35 min (purity = 94.5%).

*4.1.11. (±)-1-(6-Oxo-1,2,3,4,6,10b-hexahydropyrido[2,1-a]isoindol-10-yl)-3-(4-(((1-(2-((1,2,3,4-tetrahydroacridin-9-yl)amino)ethyl)-1H-1,2,3-triazol-4-yl)methoxy)methyl)pyridin-2-yl)urea (**(±)-2**).*

General procedure D was followed, using the alkyne **(±)-25** (74 mg) and azide **14** (51 mg). Purification by flash chromatography on silica gel (CH_2Cl_2/MeOH/NH_4OH 97:3:1, v/v/v) gave the desired compound **(±)-2** (81 mg) in 65% yield. ^{1}H NMR (300 MHz, DMSO) δ 11.21 (bs, 1H), 9.96 (s, 1H), 8.26 – 8.19 (m, 2H), 8.06 (s, 1H), 8.02 (d, *J* = 8.1 Hz, 1H), 7.74 (d, *J* = 7.5 Hz, 1H), 7.61 (t, *J* = 7.5 Hz, 1H), 7.49 – 7.32 (m, 3H), 7.26 (s, 1H), 6.95 (d, *J* = 5.3 Hz, 1H), 6.18 (bs, 1H), 4.68 – 4.58 (m, 3H), 4.56 (s, 2H), 4.49 (s, 2H), 4.28 (m, 1H), 4.01 (m, 2H), 3.04 (t, *J* =

11.5 Hz, 1H), 2.89 (t, *J* = 6.0 Hz, 2H), 2.71 (d, *J* = 13.3 Hz, 1H), 2.57 (t, *J* = 5.6 Hz, 2H), 1.91 (m, 1H), 1.75 (m, 6H), 1.25 (m, 1H), 0.88 (dd, *J* = 23.1, 10.9 Hz, 1H). ^{13}C NMR (75 MHz, DMSO) δ 164.6, 153.0, 152.2, 150.5, 146.0, 143.4, 134.8, 134.0, 132.9, 128.9, 124.7, 124.1, 123.4, 122.2, 117.3, 115.8, 115.5, 109.5, 69.4, 63.2, 57.3, 49.7, 47.5, 30.0, 25.1, 24.5, 23.0, 22.2, 21.7. (Eight carbons are missing despite an extended acquisition time, due to a DMSO peak that masks some signals). MS (ESI+): *m/z* (%): 658 (100) $[M+H]^+$. HRMS (ESI+) *m/z* calc. for $C_{37}H_{40}N_9O_3^+$ 658.3176; found 658.3228. HPLC: t_R = 22.35 min (purity = 97.8%).

*4.1.12. Methyl 4-(chloromethyl)picolinate (**20**).*

To a stirred solution of methyl 4-(hydroxymethyl)picolinate **16** (0.70 g, 4.1 mmol) in dry CH_2Cl_2 (40 mL) was added Et_3N (1.16 mL, 8.3 mmol) . The mixture was cooled to 0 °C, and mesyl chloride (0.49 mL, 6.3 mmol) was slowly added. The mixture was then heated for 24 h, and quenched at room temperature with a saturated solution of $NaHCO_3$. The aqueous layer was extracted with EtOAc (x3). The organic phase was washed with brine, dried over $MgSO_4$, filtered, and concentrated *in vacuo*. The residue was purified by silica gel chromatography (99/1 CH_2Cl_2/MeOH) to afford **20** as a brown oil in 92% yield (0.72 g). ^{1}H NMR (300 MHz, $CDCl_3$) δ 8.75 (d, *J* = 4.9 Hz, 1H), 8.16 (d, *J* = 1.0 Hz, 1H), 7.52 (dd, *J* = 5.0, 1.7 Hz, 1H), 4.61 (s, 2H), 4.03 (s, 3H). ^{13}C NMR (75 MHz, $CDCl_3$) δ 164.9, 149.9, 148.0, 147.3, 125.9, 124.1, 52.7, 43.3. MS (ESI+): *m/z* (%): 188 (33), 186 (100) $[M+H]^+$

*4.1.13. Methyl 4-((methyl(prop-2-ynyl)amino)methyl)picolinate (**21**).*

To a stirred solution of methyl 4-(chloromethyl)picolinate **20** (602 mg, 3.2 mmol) in dry CH_3CN (60 mL) were added K_2CO_3 (896 mg, 6.4 mmol) and *N*-methylpropargyl amine (0.41

mL, 4.8 mmol). The reaction mixture was refluxed for 24 h. The mixture was concentrated *in vacuo*, and water was added, followed by extraction with EtOAc (x3). The organic phase was washed with brine, dried over $MgSO_4$, filtered, and concentrated *in vacuo*. The residue was purified by chromatography on silica gel (CH_2Cl_2/MeOH 99/1, v/v) to afford **21** as a beige solid in 74% yield (524 mg). ^{1}H NMR (300 MHz, $CDCl_3$) δ 8.68 (d, *J* = 4.9 Hz, 1H), 8.12 (d, *J* = 0.8 Hz, 1H), 7.49 (m, 1H), 4.00 (s, 3H), 3.65 (s, 2H), 3.34 (d, *J* = 2.4 Hz, 2H), 2.33 (s, 3H), 2.29 (t, *J* = 2.4 Hz, 1H). ^{13}C NMR (75 MHz, $CDCl_3$) δ 165.7, 149.8, 149.4, 148.0, 126.9, 125.2, 77.6, 77.2, 76.7, 73.8, 58.5, 52.8, 45.3, 41.7. MS (ESI+): *m/z* (%): 219 (100) $[M+H]^+$.

*4.1.14. 4-((Methyl(prop-2-yn-1-yl)amino)methyl)picolinohydrazide (**22**).*

General procedure A was followed, using methyl ester **21** (195 mg, 0.9 mmol), to give **22** as a yellow solid (195 mg) in 99% yield. ^{1}H NMR (300 MHz, $CDCl_3$) δ 8.97 (s, 1H), 8.48 (dd, *J* = 4.9, 0.6 Hz, 1H), 8.13 (dd, *J* = 1.6, 0.7 Hz, 1H), 7.46 (dd, *J* = 4.9, 1.7 Hz, 1H), 4.07 (s, 2H), 3.65 (s, 2H), 3.33 (d, *J* = 2.4 Hz, 2H), 2.33 (s, 3H), 2.28 (t, *J* = 2.4 Hz, 1H). ^{13}C NMR (75 MHz, $CDCl_3$) δ 164.9, 149.8, 149.3, 148.6, 126.5, 122.5, 78.0, 73.9, 58.7, 45.5, 41.9. MS (ESI+): *m/z* (%): 219 (100) $[M+H]^+$.

*4.1.15. 4-((Methyl(prop-2-yn-1-yl)amino)methyl)picolinoyl azide (**23**).*

General procedure B was followed, using acyl hydrazine **22** (300 mg), to give the desired acyl azide **23** (260 mg) as a white solid in 83% yield. ^{1}H NMR (300 MHz, $CDCl_3$) δ 8.67 (dd, *J* = 4.9, 0.6 Hz, 1H), 8.14 (dd, *J* = 1.5, 0.7 Hz, 1H), 7.54 (dd, *J* = 4.9, 1.6 Hz, 1H), 3.67 (s, 2H), 3.34 (d, *J* = 2.4 Hz, 2H), 2.33 (s, 3H), 2.29 (t, *J* = 2.4 Hz, 1H). ^{13}C NMR (75 MHz, $CDCl_3$) δ 172.22,

150.10, 150.02, 148.21, 128.17, 124.96, 77.86, 74.02, 58.56, 45.55, 41.90. MS (ESI+): *m/z* (%): 229 (100) $[M+H]^+$.

*4.1.16. (±)-1-(4-((Methyl(prop-2-yn-1-yl)amino)methyl)pyridin-2-yl)-3-(6-oxo-1,2,3,4,6,10b-hexahydropyrido[2,1-a]isoindol-10-yl)urea (**(±)-26**).*

General procedure C was followed, using the acyl azide **23** (60 mg) and tetrahydropyrido[2,1-*a*]isoindolone **(±)-24** (53 mg). Purification by flash chromatography using (CH_2Cl_2/MeOH/NH_4OH 98:2:1, v/v/v) gave the urea **(±)-26** (96 mg) as a beige solid in 91% yield. ^{1}H NMR (300 MHz, DMSO) δ 11.29 (s, 1H), 9.90 (s, 1H), 8.24 (m, 2H), 7.46 (t, *J* = 7.7 Hz, 1H), 7.38 (dd, *J* = 7.4, 1.0 Hz, 1H), 7.27 (s, 1H), 7.01 (d, *J* = 4.5 Hz, 1H), 4.59 (dd, *J* = 11.5, 3.2 Hz, 1H), 4.27 (dd, *J* = 12.9, 4.3 Hz, 1H), 3.53 (s, 2H), 3.34 (d, *J* = 2.1 Hz, 2H), 3.23 (t, *J* = 2.1 Hz, 1H), 3.05 (td, *J* = 13.5, 3.5 Hz, 1H), 2.72 (m, 1H), 2.23 (s, 3H), 1.93 (m, 1H), 1.76 (t, *J* = 12.3 Hz, 2H), 1.33 – 1.20 (m, 1H), 0.96 – 0.82 (m, 1H). ^{13}C NMR (75 MHz, DMSO) δ 164.6, 153.1, 152.2, 150.9, 146.0, 134.8, 134.0, 132.9, 128.9, 122.1, 117.7, 117.3, 111.4, 78.6, 76.3, 58.3, 57.3, 44.9, 41.2, 30.0, 25.1, 23.1. MS (ESI+): *m/z* = 404 $[M+H]^+$. HRMS (ESI+) *m/z* calcd for $C_{23}H_{26}N_5O_2$ 404.2008; found 404.2075. HPLC: t_R = 19.40 min (purity > 98.5%).

*4.1.17. (±)-1-(4-((Methyl((1-(2-((1,2,3,4-tetrahydroacridin-9-yl)amino)ethyl)-1H-1,2,3-triazol-4-yl)methyl)amino)methyl)pyridin-2-yl)-3-(6-oxo-1,2,3,4,6,10b-hexahydropyrido[2,1-a]isoindol-10-yl)urea (**(±)-3**).*

General procedure D was followed, using alkyne **(±)-26** (74 mg) and azide **6** (49 mg). Purification by flash chromatography (CH_2Cl_2/MeOH/NH_4OH 95:5:1 v/v/v) gave **(±)-3** (88 mg) in 72% yield. ^{1}H NMR (300 MHz, DMSO) δ 13.90 (bs, 1H), 11.21 (bs, 1H), 9.89 (s, 1H), 8.21

(dd, *J* = 17.9, 6.7 Hz, 3H), 7.96 (s, 1H), 7.85 – 7.72 (m, 2H), 7.54 – 7.42 (m, 2H), 7.40 – 7.35 (m, 1H), 7.26 (s, 1H), 6.91 (d, *J* = 5.1 Hz, 1H), 4.75 – 4.72 (t, *J* = 5.2 Hz, 2H), 4.59 (dd, *J* = 11.5, 3.2 Hz, 1H), 4.29 – 4.25 (m, 3H), 3.54 (s, 2H), 3.05 (t, *J* = 11.9 Hz, 1H), 2.93 (s, 2H), 2.73 (s, 2H), 2.55 (s, 2H), 2.00 (s, 3H), 1.92 (d, *J* = 10.3 Hz, 1H), 1.76 (m, 6H), 1.31 – 1.15 (m, 2H), 0.88 (dd, *J* = 22.8, 10.9 Hz, 2H). ^{13}C NMR (75 MHz, DMSO) δ 164.6, 162.3, 155.0, 153.0, 152.2, 151.1, 146.0, 143.2, 134.8, 134.1, 132.9, 131.9, 128.8, 125.0, 124.4, 124.2, 122.1, 120.5, 117.6, 117.2, 116.6, 112.9, 111.3, 58.9, 57.3, 51.1, 49.4, 47.4, 41.5, 35.8, 30.0, 28.6, 25.1, 24.2, 23.0, 21.5, 20.5. (one carbon is missing despite an extended acquisition time). MS (ESI+): *m/z* (%): 671 (100) $[M+H]^+$. HRMS (ESI+) *m/z* calcd for $C_{38}H_{43}N_{10}O_2$ 671.3492; found 671.3583. HPLC: t_R = 20.82 min (purity > 98.3%).

*4.1.18. Methyl 4-(((1-((trimethylsilyl)methyl)-1H-1,2,3-triazol-4-yl)methoxy)methyl)picolinate (**30**).*

General procedure D was followed, using the alkyne **17** (37 mg) and trimethylsilylmethyl azide (0.29 mL). Purification by flash chromatography (CH_2Cl_2/MeOH 97:3, v/v) gave **30** (44 mg) in 74% yield. ^{1}H NMR (300 MHz, $CDCl_3$) δ 8.66 (d, *J* = 4.4 Hz, 1H), 8.07 (s, 1H), 7.44 (s, 1H), 4.71 (s, 2H), 4.64 (s, 2H), 3.98–3.88 (m, 5H), 0.11 (s, 9H). ^{13}C NMR (75 MHz, $CDCl_3$) δ 165.4, 149.6, 148.7, 147.7, 143.8, 124.8, 123.2, 123.0, 69.7, 64.0, 52.6, 41.8, -2.7. MS (ESI+): *m/z* (%): 235 (100) $[M+H]^+$.

*4.1.19. Methyl 4-(((1-methyl-1H-1,2,3-triazol-4-yl)methoxy)methyl)picolinate (**31**).*

To a solution of **30** (131 mg, 0.390 mmol) in THF (1.6 mL) was added at 0 °C TBAF (0.78 mL, 0.78 mmol, C = 1 mol/L). The solution was stirred at 0 °C for 1 h, and then at room

temperature for 24 h. A saturated solution of $NaHCO_3$ was added, followed by extraction with EtOAc (x 3). The organic phase was washed with brine, dried over $MgSO_4$, filtered, and concentrated *in vacuo* to afford **31** in 76% yield without further purification. ^{1}H NMR (300 MHz, $CDCl_3$) δ 8.68 (d, *J* = 4.9 Hz, 1H), 8.08 (d, *J* = 0.7 Hz, 1H), 7.57 (s, 1H), 7.45 (dd, *J* = 4.9, 0.8 Hz, 1H), 4.74 (s, 2H), 4.67 (s, 2H), 4.10 (s, 3H), 3.99 (s, 3H). ^{13}C NMR (75 MHz, $CDCl_3$) δ 165.5, 149.7, 148.7, 147.8, 144.3, 124.8, 123.7, 123.0, 69.8, 64.0, 52.7, 36.5. MS (ESI+): *m/z* (%): 263 (100) $[M + H]^+$

*4.1.20. 4-(((1-Methyl-1H-1,2,3-triazol-4-yl)methoxy)methyl)picolinohydrazide (**32**).*

General procedure A was followed, using methyl ester **31** (114 mg, 0.4 mmol), to give **32** as a yellow solid (114 mg) in 99% yield. ^{1}H NMR (300 MHz, $CDCl_3$) δ 8.96 (s, 1H), 8.50 (d, *J* = 5.0 Hz, 1H), 8.10 (d, *J* = 0.8 Hz, 1H), 7.59 (s, 1H), 7.44 (dd, *J* = 4.9, 1.6 Hz, 1H), 4.75 (s, 2H), 4.68 (s, 2H), 4.11 (s, 3H), 4.08 (s, 2H). ^{13}C NMR (75 MHz, $CDCl_3$) δ 164.4, 149.0, 148.9, 148.4, 144.5, 124.3, 123.8, 120.1, 70.0, 64.0, 36.6. MS (ESI+): *m/z* (%): 263 (100) $[M + H]^+$.

*4.1.21. 4-(((1-Methyl-1H-1,2,3-triazol-4-yl)methoxy)methyl)picolinoyl azide (**33**).*

General procedure B was followed, using acyl hydrazine **32** (116 mg) to give the desired acyl azide **33** (30 mg) as a white solid in 88% yield. ^{1}H NMR (300 MHz, $CDCl_3$) δ 8.68 (d, *J* = 4.9 Hz, 1H), 8.10 (s, 1H), 7.58 (s, 1H), 7.51 (d, *J* = 4.9 Hz, 1H), 4.76 (s, 2H), 4.69 (s, 2H), 4.12 (s, 3H). ^{13}C NMR (75 MHz, $CDCl_3$) δ 172.2, 150.1, 149.3, 148.2, 144.72, 126.1, 123.8, 122.9, 70.06, 64.4, 36.9. MS (ESI+): *m/z* (%): 273 (100) $[M + H]^+$.

*4.1.22. (±)-1-(4-(((1-Methyl-1H-1,2,3-triazol-4-yl)methoxy)methyl)pyridin-2-yl)-3-(6-oxo-1,2,3,4,6,10b-hexahydropyrido[2,1-a]isoindol-10-yl)urea (**(±)-27**).*

General procedure C was followed, using acyl azide **33** (26 mg) and tetrahydropyrido[2,1-*a*]isoindolone **(±)-24** (20 mg). Purification by flash chromatography using (CH_2Cl_2/MeOH/NH_4OH 97:3:1 v/v/v) gave the urea **(±)-27** (11 mg) as a white solid in 74% yield. ^{1}H NMR (300 MHz, $CDCl_3$) δ 11.93 (s, 1H), 8.25 – 8.14 (m, 3H), 7.63 (d, *J* = 7.4 Hz, 1H), 7.58 (s, 1H), 7.44 (t, *J* = 7.8 Hz, 1H), 6.95 (d, *J* = 5.4 Hz, 1H), 6.88 (s, 1H), 4.74 (s, 2H), 4.62 (s, 2H), 4.58 – 4.44 (m, 2H), 4.15 – 4.08 (m, 3H), 3.01 (td, *J* = 13.2, 3.7 Hz, 1H), 2.79 (dd, *J* = 13.1, 3.9 Hz, 1H), 2.06 – 1.98 (m, 1H), 1.83 (dd, *J* = 12.9, 2.1 Hz, 1H), 1.51 – 1.39 (m, 1H), 1.25 (s, 1H), 1.08 (ddd, *J* = 25.4, 13.0, 3.7 Hz, 1H). ^{13}C NMR (75 MHz, $CDCl_3$) δ 166.1, 153.4, 153.1, 151.1, 145.6, 144.7, 135.7, 133.5, 133.5, 129.2, 123.9, 123.8, 119.3, 116.1, 110.0, 70.2, 64.2, 58.6, 40.0, 36.9, 30.4, 25.4, 24.1. MS (ESI+): *m/z* (%): 448 (100) $[M+H]^+$. HRMS (ESI+): *m/z* calcd for $C_{23}H_{26}N_7O_3$ 448.2019; found 448.2083. HPLC: t_R = 20.15 min (purity = 96.5%).

*4.1.23. (±)-1-(6-Oxo-1,2,3,4,6,10b-hexahydropyrido[2,1-a]isoindol-10-yl)-3-(4-(((1-(3-phenylpropyl)-1H-1,2,3-triazol-4-yl)methoxy)methyl)pyridin-2-yl)urea (**(±)-28A**).*

General procedure D was followed, using the alkyne **(±)-25** (30 mg) and azide **34A** (10 mg). Purification by flash chromatography (CH_2Cl_2/MeOH/NH_4OH 95:5:1, v/v/v) gave the desired product, **(±)-28A** (33 mg), in 99% yield. ^{1}H NMR (300 MHz, DMSO) δ 11.26 (s, 1H), 9.92 (s, 1H), 8.25 – 8.21 (m, 3H), 7.45 (t, *J* = 7.7 Hz, 1H), 7.38 (d, *J* = 7.2 Hz, 1H), 7.31 – 7.26 (m, 3H), 7.22 – 7.15 (m, 3H), 7.01 (d, *J* = 5.2 Hz, 1H), 4.64 (s, 2H), 4.60 – 4.53 (m, 3H), 4.37 (t, *J* = 7.1 Hz, 2H), 4.26 (dd, *J* = 12.6, 4.1 Hz, 1H), 3.09 – 3.00 (m, 1H), 2.71 (d, *J* = 12.1 Hz, 1H), 2.61 – 2.53 (m, 2H), 2.21 – 2.07 (m, 2H), 1.91 (d, *J* = 13.1 Hz, 1H), 1.75 (t, *J* = 12.9 Hz, 2H), 1.26 (d, *J*

= 13.6 Hz, 1H), 0.95 – 0.83 (m, 1H). ^{13}C NMR (75 MHz, DMSO) δ 164.6, 153.1, 152.1, 150.6, 146.0, 143.5, 140.7, 134.8, 133.9, 132.9, 128.9, 128.4, 128.3, 126.0, 124.1, 122.1, 117.3, 115.8, 109.5, 69.5, 63.4, 57.3, 48.9, 31.9, 31.3, 30.0, 25.1, 23.0. (One aliphatic carbon is missing despite an extended acquisition time, perhaps due to a DMSO peak which masks the signal). MS (ESI+): m/z (%): 552 (100) $[M+H]^+$. HRMS (ESI+): *m/z* calcd for $C_{31}H_{34}N_7O_3$ 552.2645; found 552.2708. HPLC: t_R = 25.67 min (purity > 95.0%).

*4.1.24. (±)-1-(6-Oxo-1,2,3,4,6,10b-hexahydropyrido[2,1-a]isoindol-10-yl)-3-(4-(((1-(2-(pyridin-4-ylamino)ethyl)-1H-1,2,3-triazol-4-yl)methoxy)methyl)pyridin-2-yl)urea (**(±)-28B**).*

General procedure D was followed, using the alkyne **(±)-25** (26 mg) and azide **34B** (11 mg). Purification by flash chromatography on silica gel (CH_2Cl_2/MeOH/NH_4OH 95:5:1, v/v/v) gave the desired compound **(±)-28B** (15 mg) in 41% yield. ^{1}H NMR (300 MHz, DMSO) δ 11.23 (s, 1H), 9.94 (s, 1H), 8.24 (d, *J* = 5.4 Hz, 2H), 8.18 (s, 1H), 8.02 (d, *J* = 5.5 Hz, 2H), 7.51 – 7.37 (m, 2H), 7.28 (s, 1H), 6.99 (d, *J* = 4.9 Hz, 1H), 6.90 (t, *J* = 5.5 Hz, 1H), 6.54 (d, *J* = 6.2 Hz, 2H), 4.62 (s, 2H), 4.58 – 4.50 (m, 4H), 4.27 (dd, *J* = 13.7, 5.2 Hz, 1H), 3.62 (dd, *J* = 11.9, 5.8 Hz, 2H), 3.09 – 2.99 (m, 1H), 2.71 (d, *J* = 10.8 Hz, 1H), 1.92 (d, *J* = 9.7 Hz, 1H), 1.75 (t, *J* = 13.1 Hz, 2H), 1.31 – 1.24 (m, 2H), 0.95 – 0.83 (m, 1H). ^{13}C NMR (75 MHz, DMSO) δ 164.6, 162.5, 153.9, 153.1, 152.2, 150.5, 148.0, 146.0, 143.5, 134.8, 134.0, 132.9, 128.9, 124.6, 122.2, 117.3, 115.8, 109.5, 107.2, 69.5, 63.3, 57.3, 48.4, 41.7, 30.0, 25.1, 23.0. MS (ESI+): *m/z* (%): 554 (100) $[M+H]^+$. HRMS (ESI+): *m/z* calcd for $C_{29}H_{32}N_9O_3$ 554.2550; found 554.2631. HPLC: t_R = 19.95 min (purity = 96.2%).

*4.1.25. ((±))-1-(6-Oxo-1,2,3,4,6,10b-hexahydropyrido[2,1-a]isoindol-10-yl)-3-(4-(((1-(2-(quinolin-4-ylamino)ethyl)-1H-1,2,3-triazol-4-yl)methoxy)methyl)pyridin-2-yl)urea (**(±)-28C**).*

General procedure D was followed, using the alkyne **(±)-25** (25 mg) and azide **34C** (17 mg). Purification by flash chromatography (CH_2Cl_2/MeOH/NH_4OH 95:5:1 v/v/v) gave the desired compound **(±)-28C** (18 mg) in 47% yield. ^{1}H NMR (300 MHz, DMSO) δ 11.27 (bs, 1H), 9.97 (s, 1H), 8.38 (d, *J* = 5.4 Hz, 1H), 8.22 (dd, *J* = 14.0, 8.7 Hz, 3H), 8.10 (d, *J* = 8.4 Hz, 1H), 7.79 (d, *J* = 8.6 Hz, 1H), 7.60 (t, *J* = 7.1 Hz, 1H), 7.49 – 7.36 (m, 3H), 7.30 (t, *J* = 5.8 Hz, 1H), 7.25 (s, 1H), 6.95 (d, *J* = 5.3 Hz, 1H), 6.50 (d, *J* = 5.4 Hz, 1H), 4.67 (t, *J* = 6.1 Hz, 2H), 4.62 – 4.55 (m, 3H), 4.52 (s, 2H), 4.27 (d, *J* = 9.0 Hz, 1H), 3.80 (dd, *J* = 11.8, 5.8 Hz, 2H), 3.05 (t, *J* = 11.8 Hz, 1H), 2.71 (d, *J* = 10.5 Hz, 1H), 1.92 (d, *J* = 13.0 Hz, 1H), 1.75 (t, *J* = 13.1 Hz, 2H), 1.27 (dd, *J* = 18.4, 6.0 Hz, 1H), 0.97 – 0.82 (m, 1H). ^{13}C NMR (75 MHz, DMSO) δ 164.6, 153.1, 152.2, 150.7, 150.6, 149.4, 148.3, 145.9, 143.4, 134.8, 134.0, 132.9, 129.1, 128.9, 128.8, 124.7, 124.0, 122.1, 121.5, 118.8, 117.3, 115.7, 109.4, 98.3, 69.4, 63.3, 57.3, 47.9, 42.4, 29.9, 25.6, 23.1. (One carbon is missing despite an extended acquisition time). MS (ESI+): *m/z* (%): 603 (100) $[M + H]^+$. HRMS (ESI+): *m/z* calcd for $C_{33}H_{34}N_9O_3$ 604.2706; found 604.2805. HPLC: t_R = 21.07 min (purity = 96.4%).

*4.1.26. N-(2-(4-(Trimethylsilyl)-1H-1,2,3-triazol-1-yl)ethyl)-1,2,3,4-tetrahydroacridin-9-amine (**35**).*

To a solution of alkyne **14** (80 mg, 0.3 mmol) in DMF (3.7 mL) were added $CuSO_4.5H_2O$ (22 mg, 0.09 mmol), sodium ascorbate (36 mg, 0.18 mmol) and trimethylsilylacetylene (0.06 mL, 0.44 mmol). The mixture was stirred at room temperature for 3 h. It was then concentrated *in vacuo*, and purified by flash chromatography on silica gel (CH_2Cl_2/MeOH/NH_4OH 98.5:1.5:1, v/v/v), to give the desired compound **35**, as a yellow oil in 99% (109 mg) yield. ^{1}H NMR (300

MHz, $CDCl_3$) δ 7.91 (d, *J* = 7.8 Hz, 1H), 7.75 (d, *J* = 7.7 Hz, 1H), 7.56 (ddd, *J* = 8.3, 6.8, 1.3 Hz, 1H), 7.39 – 7.32 (m, 2H), 4.58 – 4.47 (m, 2H), 4.01 (dd, *J* = 10.8, 6.9 Hz, 2H), 3.06 (t, *J* = 6.3 Hz, 2H), 2.60 (t, *J* = 6.1 Hz, 2H), 1.96 – 1.79 (m, 4H), 0.31 (s, 9H). ^{13}C NMR (75 MHz, $CDCl_3$) δ 158.8, 149.0, 147.2, 146.8, 129.8, 128.8, 128.3, 124.2, 122.0, 120.6, 118.0, 50.0, 47.9, 34.0, 24.8, 22.9, 22.7, -1.23.

*4.1.27. N-(2-(1H-1,2,3-triazol-1-yl)ethyl)-1,2,3,4-tetrahydroacridin-9-amine (**29**).*

To a solution of *N*-(2-(4-(trimethylsilyl)-1*H*-1,2,3-triazol-1-yl)ethyl)-1,2,3,4-tetrahydroacridin-9-amine. **35** (100 mg, 0.27 mmol) in THF (1.4 mL) was added TBAF (1 M in THF, 0.54 mL, 0.55 mmol), followed by reflux for 3 h. After cooling, the reaction was quenched with water. The aqueous layer was extracted with EtOAc (x3). The organic layer was dried over $MgSO_4$, filtered, and concentrated *in vacuo* to afford **29** as a white solid in 50% yield (40 mg), without further purification. ^{1}H NMR (300 MHz, $CDCl_3$) δ 7.91 (dd, *J* = 8.5, 0.7 Hz, 1H), 7.74 (dd, *J* = 8.5, 0.8 Hz, 1H), 7.72 (d, *J* = 0.9 Hz, 1H), 7.55 (ddd, *J* = 8.3, 6.8, 1.3 Hz, 1H), 7.45 (d, *J* = 0.9 Hz, 1H), 7.35 (ddd, *J* = 8.2, 6.8, 1.2 Hz, 1H), 4.58 – 4.48 (m, 2H), 4.44 (bs, 1H), 3.99 (d, *J* = 5.0 Hz, 2H), 3.05 (t, *J* = 6.2 Hz, 2H), 2.58 (t, *J* = 6.1 Hz, 2H), 1.95 – 1.78 (m, 4H). ^{13}C NMR (75 MHz, $CDCl_3$) δ 159.1, 149.0, 147.5, 134.2, 129.2, 128.6, 124.5, 124.4, 122.1, 120.8, 118.4, 50.7, 46.0, 34.2, 24.9, 23.0, 22.9. HPLC: t_R = 18.77 min (purity = 96.6%).

*4.1.28. Methyl 4-formylpicolinate (**38**).*

To a stirred solution of methyl 4-(hydroxymethyl)picolinate, **16** (605 mg, 3.62 mmol) in EtOAc (36 mL), IBX (3.04 g, 10.85 mmol) was added, followed by reflux for 3 h. The mixture was then cooled to room temperature, filtered, and the solid washed with EtOAc. The filtrate was concentrated to afford **38** as a pale yellow solid in quantitative yield (597 mg). ^{1}H NMR (300

MHz, $CDCl_3$) δ 10.15 (s, 1H), 9.01 (d, *J* = 5.2 Hz, 1H), 8.52 (dd, *J* = 1.5, 0.9 Hz, 1H), 7.90 (dd, *J* = 4.8, 1.5 Hz, 1H), 4.05 (s, 3H). ^{13}C NMR (75 MHz, $CDCl_3$) δ 190.5, 164.8, 151.4, 149.8, 142.8, 125.0, 124.0, 53.3. MS (ESI+): *m/z* (%): 165 (100) $[M+H]^+$.

*4.1.29. Methyl 4-ethynylpicolinate (**41**).*

To a stirred solution of methyl 4-formylpicolinate, **38** (657 mg, 3.98 mmol) in dry MeOH (47.5 mL) were added successively K_2CO_3 (1.1 g, 7.96 mmol) and dimethyl (1-diazo-2-oxopropyl)phosphonate (1.15 g, 5.97 mmol). The mixture was stirred for 1 h, and concentrated *in vacuo*. Water was added, and the aqueous layer was extracted with CH_2Cl_2 (x3). The organic phase was dried over $MgSO_4$, filtered, and concentrated under reduced pressure. The residue was purified by chromatography on silica gel (CH_2Cl_2/EtOAc 90/10, v/v) to afford **41** as a grey solid in 36% yield (234 mg). ^{1}H NMR (300 MHz, $CDCl_3$) δ 8.68 (dd, *J* = 4.9, 0.8 Hz, 1H), 8.12 (dd, *J* = 1.4, 0.8 Hz, 1H), 7.48 (dd, *J* = 4.9, 1.6 Hz, 1H), 3.96 (s, 3H), 3.37 (s, 1H). ^{13}C NMR (75 MHz, $CDCl_3$) δ 165.1, 149.9, 148.2, 131.8, 129.2, 127.61, 83.4, 80.2, 53.1. MS (ESI+): *m/z* (%): 162 (100) $[M+H]^+$.

*4.1.30. 4-Ethynylpicolinohydrazide (**43**).*

General procedure A was followed using methyl ester **41** (325mg, 2.02 mmol) to give **43** as a white solid (325 mg) in 99% yield. ^{1}H NMR (300 MHz, DMSO) δ 9.96 (s, 1H), 8.63 (d, *J* = 4.9 Hz, 1H), 7.93 (s, 1H), 7.63 (dd, *J* = 4.9, 1.5 Hz, 1H), 4.72 (s, 1H), 4.59 (s, 2H). ^{13}C NMR (75 MHz, DMSO) δ 161.8, 150.3, 149.1, 131.1, 128.0, 123.5, 86.6, 80.5. MS (ESI+): *m/z* (%): 162 (100) $[M+H]^+$.

*4.1.31. 4-Ethynylpicolinoyl azide (**45**).*

General procedure B was followed, using acyl hydrazine **43** (325 mg, 2.02) to give the desired acyl azide **45** (285 mg) as an off-white solid in 82% yield. ^{1}H NMR (300 MHz, $CDCl_3$) δ 8.71 (dd, *J* = 4.9, 0.8 Hz, 1H), 8.19 (s, 1H), 7.57 (dd, *J* = 4.9, 1.5 Hz, 1H), 3.41 (s, 1H). ^{13}C NMR (75 MHz, $CDCl_3$) δ 171.5, 150.1, 148.3, 132.2, 130.2, 127.2, 83.9, 79.9. MS (ESI+): m/z (%): 172 (100) $[M+H]^+$.

*4.1.32. (±)-1-(4-Ethynylpyridin-2-yl)-3-(6-oxo-1,2,3,4,6,10b-hexahydropyrido[2,1-a]isoindol-10-yl)urea (**(±)-47**).*

General procedure C was followed, using the acyl azide **45** (68 mg, 0.40 mmol) and tetrahydropyrido[2,1-*a*]isoindolone **(±)-24** (80 mg, 0.40 mmol). Purification by flash chromatography on silica gel using (CH_2Cl_2/MeOH 98:2, v/v) gave the urea **(±)-47** (126 mg) as an off-white solid in 92% yield. ^{1}H NMR (300 MHz, DMSO) δ 10.67 (s, 1H), 9.97 (s, 1H), 8.30 (d, *J* = 5.2 Hz, 1H), 8.19 (dd, *J* = 7.8, 1.0 Hz, 1H), 7.46 (m, 2H), 7.39 (dd, *J* = 7.4, 1.1 Hz, 1H), 7.11 (dd, *J* = 5.2, 1.3 Hz, 1H), 4.57 (dd, *J* = 11.5, 3.2 Hz, 1H), 4.26 (dd, *J* = 13.0, 4.2 Hz, 1H), 3.04 (td, *J* = 12.6, 2.7 Hz, 1H), 2.66 (d, *J* = 10.3 Hz, 1H), 1.91 (d, *J* = 13.1 Hz, 1H), 1.71 (m, 2H), 1.34 – 1.19 (m, *J* = 18.5, 10.4 Hz, 2H), 0.96 – 0.79 (m, 1H). ^{13}C NMR (75 MHz, DMSO) δ 164.54, 153.0, 151.9, 147.1, 135.0, 133.7, 132.9, 132.0, 128.8, 122.4, 119.5, 117.5, 114.04, 85.6, 80.9, 57.3, 30.0, 25.0, 23.0. MS (ESI+): *m/z* (%): 692 (65) $[2M + H]^+$, 347 (100) $[M+H]^+$. HRMS (ESI+) *m/z* calcd for $C_{20}H_{19}N_4O_2^+$ 347.1430; found 347.1487. HPLC: t_R = 23.97 min (purity > 95.0%).

*4.1.33. (-)-(R)-1-(4-Ethynylpyridin-2-yl)-3-(6-oxo-1,2,3,4,6,10b-hexahydropyrido[2,1-a]isoindol-10-yl)urea (**(-)-(R)-47**).*

General procedure C was followed, using the acyl azide **45** (60 mg, 0.35 mmol) and tetrahydropyrido[2,1-*a*]isoindolone **(*R*)-24** (70 mg, 0.35 mmol). Purification by flash chromatography on silica gel using (CH_2Cl_2/MeOH 98:2, v/v) gave the urea **(*R*)-47** (87 mg) as an off-white solid in 73% yield. NMR and MS spectra were in accordance with those reported above. $[\alpha]_D^{25}$ = -150° (*c* = 0.83, DMF).

*4.1.34. (+)-(S)-1-(4-Ethynylpyridin-2-yl)-3-(6-oxo-1,2,3,4,6,10b-hexahydropyrido[2,1-a]isoindol-10-yl)urea (**(+)-(S)-47**).*

General procedure C was followed, using the acyl azide **45** (60 mg, 0.35 mmol) and tetrahydropyrido[2,1-*a*]isoindolone **(*S*)-24** (70 mg, 0.35 mmol). Purification by flash chromatography on silica gel using (CH_2Cl_2/MeOH 98:2, v/v) gave the urea **(*S*)-47** (91 mg) as an off-white solid in 76% yield. NMR and MS spectra were in accordance with those reported above. $[\alpha]_D^{25}$ = +150° (*c* = 0.83, DMF).

*4.1.35. Methyl 4-(3-oxopropyl)picolinate (**40**).*

To a stirred solution of methyl 4-(3-hydroxypropyl)picolinate **37** (1.04 g, 5.34 mmol) in EtOAc (40 mL) was added IBX (4.49 g, 16 mmol). The mixture was stirred under reflux for 12 h. It was then cooled to room temperature and filtered. The solid was washed with EtOAc. The filtrate was concentrated *in vacuo* to afford **31** as a colorless oil in 99% yield (1.02 g). The crude product was used in the next reaction without further purification. ^{1}H NMR (300 MHz, $CDCl_3$) δ 9.83 (t, *J* = 0.8 Hz, 1H), 8.64 (d, *J* = 5.0 Hz, 1H), 7.99 (d, *J* = 1.7 Hz, 1H), 7.33 (dd, *J* = 5.0, 1.8 Hz, 1H), 4.00 (s, 3H), 3.03 (t, *J* = 7.2 Hz, 2H), 2.88 (t, *J* = 7.2 Hz, 2H). ^{13}C NMR (75 MHz,

$CDCl_3$) δ 199.8, 165.6, 151.1, 149.9, 148.0, 127.1, 125.1, 52.9, 43.6, 27.1. MS (ESI+): *m/z* (%): 194 (100) $[M+H]^+$.

*4.1.36. Methyl 4-(but-3-ynyl)picolinate (**42**).*

To a stirred solution of aldehyde **40** (0.5 g, 2.59 mmol) in dry MeOH (31 mL) were added successively K_2CO_3 (715 mg, 5.18 mmol) and dimethyl (1-diazo-2-oxopropyl)phosphonate (746 mg, 3.88 mmol). The mixture was stirred for 3 h at room temperature, and then concentrated *in vacuo*. Water was added, and the product was extracted with CH_2Cl_2 (x2). The organic phase was dried over $MgSO_4$, filtered, and concentrated under reduced pressure. The residue was purified by chromatography on silica gel (CH_2Cl_2/EtOAc 90/10, v/v) to afford **42** as a pink solid in 48% yield (237 mg). ^{1}H NMR (300 MHz, $CDCl_3$) δ 8.62 (dd, *J* = 4.9, 0.5 Hz, 1H), 8.00 (d, *J* = 1.0 Hz, 1H), 7.34 (dd, *J* = 4.9, 1.8 Hz, 1H), 3.97 (s, 3H), 2.88 (t, *J* = 7.2 Hz, 2H), 2.52 (td, *J* = 7.2, 2.6 Hz, 2H), 1.96 (t, *J* = 2.6 Hz, 1H). ^{13}C NMR (75 MHz, $CDCl_3$) δ 165.9, 150.6, 149.9, 148.0, 127.2, 125.4, 82.2, 70.1, 53.0, 33.9, 19.3. MS (ESI+): *m/z* (%): 190 (100) $[M+H]^+$.

*4.1.37. 4-(But-3-yn-1-yl)picolinohydrazide (**44**).*

General procedure A was followed, using methyl ester **42** (237 mg, 1.25 mmol), to give **44** as a beige solid (114 mg) in 99% yield. ^{1}H NMR (300 MHz, $CDCl_3$) δ 9.07 (s, 1H), 8.43 (dd, *J* = 5.0, 0.6 Hz, 1H), 8.01 (dd, *J* = 1.7, 0.6 Hz, 1H), 7.30 (dd, *J* = 5.0, 1.8 Hz, 1H), 4.08 (s, 2H), 2.88 (t, *J* = 7.2 Hz, 2H), 2.52 (td, *J* = 7.2, 2.6 Hz, 2H), 1.97 (t, *J* = 2.6 Hz, 1H). ^{13}C NMR (75 MHz, $CDCl_3$) δ 164.9, 150.9, 149.2, 148.5, 126.7, 122.4, 82.4, 70.1, 34.0, 19.3. MS (ESI+): *m/z* (%): 191 (100) $[M+H]^+$.

*4.1.38. 4-(But-3-yn-1-yl)picolinoyl azide (**46**).*

General procedure B was followed, using acyl hydrazine **44** (223 mg) to give the desired acyl azide **46** (196 mg) as a white solid in 83% yield. ^{1}H NMR (300 MHz, $CDCl_3$) δ 8.63 (dd, *J* = 4.9, 0.5 Hz, 1H), 8.03 (d, *J* = 1.0 Hz, 1H), 7.42 (dd, *J* = 4.9, 1.7 Hz, 1H), 2.91 (t, *J* = 7.1 Hz, 2H), 2.55 (td, *J* = 7.1, 2.6 Hz, 2H), 1.98 (t, *J* = 2.6 Hz, 1H). ^{13}C NMR (75 MHz, $CDCl_3$) δ 172.3, 151.0, 150.0, 148.1, 128.4, 125.1, 82.1, 70.4, 33.8, 19.3. MS (ESI+): *m/z* (%): 200 (100) $[M+H]^+$.

*4.1.39. (±)-1-(4-(But-3-yn-1-yl)pyridin-2-yl)-3-(6-oxo-1,2,3,4,6,10b-hexahydropyrido[2,1-a]isoindol-10-yl)urea (**(±)-48**).*

General procedure C was followed by using the acyl azide **46** (86 mg) and tetrahydropyrido[2,1-*a*]isoindolone **(±)-24** (87 mg). Purification by flash chromatography using (CH_2Cl_2/MeOH/NH_4OH 98:2:1 v/v/v) gave the urea **(±)-48** (64 mg) as a white solid in 40% yield. ^{1}H NMR (300 MHz, DMSO) δ 11.34 (s, 1H), 9.89 (s, 1H), 8.26 (d, *J* = 7.8 Hz, 1H), 8.20 (d, *J* = 5.3 Hz, 1H), 7.45 (t, *J* = 7.7 Hz, 1H), 7.38 (d, *J* = 6.6 Hz, 1H), 7.15 (s, 1H), 7.01 (d, *J* = 5.2 Hz, 1H), 4.58 (dd, *J* = 11.5, 3.0 Hz, 1H), 4.27 (dd, *J* = 12.7, 3.9 Hz, 1H), 3.05 (td, *J* = 12.9, 2.7 Hz 1H), 2.82 (t, *J* = 2.5 Hz, 1H), 2.79 – 2.69 (m, 3H), 2.00 – 1.89 (m, 1H), 1.73 (m, 2H), 1.21 (m, 1H), 0.97 – 0.81 (m, 1H). ^{13}C NMR (75 MHz, $CDCl_3$) δ 164.6, 153.0, 152.3, 152.1, 145.8, 134.8, 134.01, 132.9, 128.9, 122.1, 118.1, 117.3, 111.7, 83.2, 72.2, 57.3, 33.4, 30.0, 25.1, 23.1, 18.4. MS (ESI+): *m/z* (%): 375 $[M + H]^+$. HRMS (ESI+) *m/z* calcd for $C_{22}H_{23}N_4O_2$ 375.1743; found 375.1815. HPLC: t_R = 21.28 min (purity = 95.3%).

4.1.40. (±)-1-(6-Oxo-1,2,3,4,6,10b-hexahydropyrido[2,1-a]isoindol-10-yl)-3-(4-(2-(1-(2-((1,2,3,4-tetrahydroacridin-9-yl)amino)ethyl)-1H-1,2,3-triazol-4-yl)ethyl)pyridin-2-yl)urea ***((±)-4)****.*

General procedure D was followed, using the alkyne (±)-**48** (64 mg) and azide **14** (46 mg). Purification by flash chromatography on silica gel (CH_2Cl_2/MeOH/NH_4OH 95:5:1, v/v/v) gave the desired compound (±)-**4** (21 mg) as a white solid, in 19% yield. ^{1}H NMR (300 MHz, $CDCl_3$) δ 11.94 (s, 1H), 8.76 (s, 1H), 8.22 (d, *J* = 7.8 Hz, 1H), 8.05 (d, *J* = 5.3 Hz, 1H), 7.88 (d, *J* = 8.3 Hz, 1H), 7.69 (d, *J* = 8.3 Hz, 1H), 7.59 (d, *J* = 7.0 Hz, 1H), 7.52 (t, *J* = 7.5 Hz, 1H), 7.44 (t, *J* = 7.8 Hz, 1H), 7.31 (d, *J* = 8.1 Hz, 1H), 7.12 (s, 1H), 6.82 (d, *J* = 5.3 Hz, 1H), 6.74 (s, 1H), 4.56 – 4.39 (m, 4H), 3.98 – 3.93 (m, 2H), 2.98 (m, 7H), 2.76 (d, *J* = 10.3 Hz, 1H), 2.61 (t, *J* = 5.9 Hz, 2H), 1.99 (d, *J* = 13.8 Hz, 1H), 1.88 – 1.79(m, 6H), 1.79 – 1.59 (m, 1H), 1.49 – 1.37 (m, 1H), 1.04 (dd, *J* = 22.2, 12.2 Hz, 1H). ^{13}C NMR (75 MHz, $CDCl_3$) δ 166.1, 159.1, 153.6, 153.5, 153.1, 149.2, 147.3, 146.5, 145.5, 135.7, 133.5, 133.5, 129.2, 129.0, 128.6, 124.5, 123.8, 122.1, 122.0, 120.7, 119.2, 118.4, 118.2, 111.9, 58.6, 50.9, 48.0, 40.0, 34.7, 34.1, 31.1, 25.8, 25.4, 25.1, 24.1, 23.0, 22.8. MS (ESI+): *m/z* (%): 642 (100) $[M+H]^+$. HRMS (ESI+): *m/z* calcd for $C_{37}H_{40}N_9O_2$ 642.3227; found 642.3329. HPLC: t_R = 21.62 min (purity = 95.7%).

4.1.41. (±)-1-(6-oxo-1,2,3,4,6,10b-hexahydropyrido[2,1-a]isoindol-10-yl)-3-(4-(1-(2-((1,2,3,4-tetrahydroacridin-9-yl)amino)ethyl)-1H-1,2,3-triazol-4-yl)pyridin-2-yl)urea ***((±)-6)****.*

General procedure D was followed, using the alkyne **(±)-47** (97 mg, 0.28 mmol) and azide **14** (75 mg, 0.28mmol). Purification by flash chromatography on silica gel (CH_2Cl_2/MeOH/NH_4OH 97:3:1, v/v/v) gave the desired compound **(±)-6** (30 mg) as an off-white solid in 18% yield. ^{1}H NMR (300 MHz, DMSO) δ 11.06 (bs, 1H), 10.01 (s, 1H), 8.62 (s, 1H), 8.32 (d, *J* = 5.4 Hz, 1H),

8.25 (d, *J* = 7.3 Hz, 1H), 8.04 – 7.94 (m, 1H), 7.80 (s, 1H), 7.72 (d, *J* = 8.1 Hz, 1H), 7.61 – 7.54 (m, 1H), 7.47 (t, *J* = 7.6 Hz, 1H), 7.42 – 7.31 (m, 3H), 5.95 (bs, 1H), 4.72 – 4.56 (m, 3H), 4.28 (d, *J* = 9.6 Hz, 1H), 4.00 (d, *J* = 5.3 Hz, 1H), 3.05 (t, *J* = 11.3 Hz, 1H), 2.87 (s, 3H), 2.73 (s, 2H), 2.61 (s, 2H), 1.91 (s, 1H), 1.77 (s, 5H), 1.33 – 1.19 (m, 1H), 0.90 (dd, *J* = 23.2, 10.2 Hz, 1H). ^{13}C NMR (75 MHz, DMSO) δ 164.6, 157.1, 153.6, 152.1, 150.3, 147.0, 143.6, 140.5, 134.9, 134.0, 132.9, 128.9, 128.7, 127.0, 124.2, 123.8, 123.0, 122.2, 119.8, 117.4, 116.5, 113.9, 107.1, 57.3, 50.2, 47.4, 35.8, 32.7, 30.0, 25.1, 24.8, 23.1, 22.4, 22.0. (one carbon is missing despite an extended acquisition time). MS (ESI+): *m/z* (%): 614 (100) $[M+H]^+$. HRMS (ESI+): *m/z* calcd for $C_{35}H_{36}N_9O_2$ 614.2914; found 614.2971. HPLC: t_R = 22.97 min (purity > 95.0%).

4.1.42. (-)-(R)-1-(6-oxo-1,2,3,4,6,10b-hexahydropyrido[2,1-a]isoindol-10-yl)-3-(4-(1-(2-((1,2,3,4-tetrahydroacridin-9-yl)amino)ethyl)-1H-1,2,3-triazol-4-yl)pyridin-2-yl)urea ***((-)-(R)-6****).*

General procedure D was followed, using the alkyne **(*R*)-47** (55 mg, 0.15 mmol) and azide **14** (38 mg, 0.15 mmol). Purification by flash chromatography on silica gel (CH_2Cl_2/MeOH/NH_4OH 97:3:1, v/v/v) gave the desired compound **(*R*)-6** (50 mg) as an off-white solid in 56% yield. NMR and MS spectra were in accordance with those reported above. $[\alpha]_D^{25}$ = -81° (*c* = 0.83, DMF).

4.1.43. (+)-(S)-1-(6-oxo-1,2,3,4,6,10b-hexahydropyrido[2,1-a]isoindol-10-yl)-3-(4-(1-(2-((1,2,3,4-tetrahydroacridin-9-yl)amino)ethyl)-1H-1,2,3-triazol-4-yl)pyridin-2-yl)urea ***((+)-(S)-6****).*

General procedure D was followed, using the alkyne **(*S*)-47** (55 mg, 0.15 mmol) and azide **14** (38 mg, 0.15 mmol). Purification by flash chromatography on silica gel (CH_2Cl_2/MeOH/NH_4OH

97:3:1, v/v/v) gave the desired compound **(*S*)-6** (40 mg) as an off-white solid in 45% yield. NMR and MS spectra were in accordance with those reported above. $[\alpha]_D^{25}$ = +81° (*c* = 0.83, DMF).

*4.1.44. Methyl 5-((trimethylsilyl)ethynyl)picolinate (**51**).*

To a solution of methyl 5-bromopyridine-2-carboxylate, **49** (1 g, 4.63 mmol) in THF (15 mL) (degassed under argon) were added dichlorobis(triphenylphosphine)palladium (0.163 mg, 0.23 mmol), CuI (88 mg, 0.46 mmol), Et_3N (15 mL) and ethynyltrimethylsilane (1.98 mL, 13.89 mmol). The stirred mixture was heated at 60 °C for 5 h. The mixture was then filtered on Celite®. The filtrate was concentrated under reduced pressure, and the residue was purified by silica gel chromatography 90/10 (petroleum ether/EtOAc) to afford **51** (1.05 g) as a brown oil in 97% yield. ^{1}H NMR (300 MHz, $CDCl_3$) δ 9.10 (d, *J* = 2.0 Hz, 1H), 8.81 (d, *J* = 2.1 Hz, 1H), 8.32 (t, *J* = 2.1 Hz, 1H), 3.95 (s, 3H), 0.26 (s, 9H). ^{13}C NMR (75 MHz, $CDCl_3$) δ 165.2, 155.9, 149.6, 139.8, 125.5, 120.4, 100.4, 99.8, 52.6, -0.2. MS (ESI+): *m/z* (%): 234 (100) $[M+H]^+$.

*4.1.45. Methyl 5-ethynylpicolinate (**53**).*

To a solution of methyl 5-((trimethylsilyl)ethynyl)picolinate **51** (1 g, 4.23 mmol) in a mixture of CH_2Cl_2/MeOH (26 mL, 50:50, v/v) was added KF (0.74 g, 12.7 mmol). The reaction mixture was stirred at room temperature overnight, and then filtered and concentrated *in vacuo*. The residue was purified by silica gel chromatography (petroleum ether/EtOAc, 80/20) to afford **53** (528 mg) as a brown solid in 77% yield. ^{1}H NMR (300 MHz, $CDCl_3$) δ 9.15 (d, *J* = 2.0 Hz, 1H), 8.86 (d, *J* = 2.1 Hz, 1H), 8.37 (t, *J* = 2.1 Hz, 1H), 3.97 (s, 3H), 3.27 (s, 1H). ^{13}C NMR (75 MHz, $CDCl_3$) δ 165.1, 156.1, 150.1, 140.1, 125.7, 119.4, 81.9, 79.4, 52.7. MS (ESI+): *m/z* (%): 162 (100) $[M+H]^+$.

*4.1.46. 5-Ethynylpicolinohydrazide (**55**).*

General procedure A was followed, using methyl ester **53** (623 mg, 3.87 mmol), to give **55** as an orange solid (623 mg) in 99% yield. ^{1}H NMR (300 MHz, DMSO) δ 10.02 (s, 1H), 8.95 (d, *J* = 2.1 Hz, 1H), 8.79 (d, *J* = 2.0 Hz, 1H), 8.22 (t, *J* = 2.1 Hz, 1H), 4.59 (s, 2H), 3.31 (s, 1H). ^{13}C NMR (75 MHz, DMSO) δ 163.3, 153.9, 147.7, 137.2, 128.5, 118.5, 84.9, 79.8. MS (ESI+): *m/z* (%): 162 (100) $[M+H]^+$.

*4.1.47. 5-Ethynylpicolinoyl azide (**57**).*

General procedure B was followed using acyl hydrazine **55** (572 mg, 3.55 mmol) to give the desired acyl azide **57** (588 mg) as an off-white solid in 96% yield. ^{1}H NMR (300 MHz, $CDCl_3$) δ 9.14 (d, *J* = 2.0 Hz, 1H), 8.90 (d, *J* = 2.0 Hz, 1H), 8.35 (t, *J* = 2.0 Hz, 1H), 3.30 (s, 1H). ^{13}C NMR (75 MHz, $CDCl_3$) δ 170.7, 157.2, 149.7, 139.7, 126.2, 119.8, 82.4, 79.1. MS (ESI+): *m/z* (%): 173 (100) $[M+H]^+$.

*4.1.48. (±)-1-(5-Ethynylpyridin-2-yl)-3-(6-oxo-1,2,3,4,6,10b-hexahydropyrido[2,1-a]isoindol-10-yl)urea (**(±)-59**).*

General procedure C was followed, using the acyl azide **57** (68 mg, 0.44 mmol) and tetrahydropyrido[2,1-*a*]isoindolone tetrahydropyrido[2,1-*a*]isoindolone **(±)-24** (80 mg, 0.44 mmol). Purification by flash chromatography on silica gel using (CH_2Cl_2/MeOH/NH_4OH 96:4:1, v/v/v) gave the urea **(±)-59** (81 mg) as a white solid in 65% yield. ^{1}H NMR (300 MHz, $CDCl_3$) δ 8.74 (s, 1H), 8.41 (d, *J* = 2.5 Hz, 1H), 8.35 (d, *J* = 1.7 Hz, 1H), 8.25 (s, 1H), 8.23 – 8.20 (m, 1H),

7.73 (d, *J* = 7.8 Hz, 1H), 7.54 (d, *J* = 7.0 Hz, 1H), 7.39 (t, *J* = 7.7 Hz, 1H), 4.55 (dd, *J* = 11.6, 3.4 Hz, 1H), 4.43 (d, *J* = 9.6 Hz, 1H), 2.97 (dt, *J* = 12.0, 1H), 2.59 (d, *J* = 10.4 Hz, 1H), 1.84 (dd, *J* = 26.3, 13.0 Hz, 3H), 1.50 (m, 1H), 1.34 (m, 1H), 1.00 (m, 1H). ^{13}C NMR (75 MHz, $CDCl_3$) δ 166.8, 152.9, 146.8, 139.9, 137.3, 135.7, 133.6, 133.1, 129.6, 129.0, 125.8, 119.7, 119.4, 81.0, 80.3, 59.6, 40.3, 30.2, 25.5, 23.5. MS (ESI+): *m/z* (%): 347 (100) $[M + H]^+$. HRMS (ESI+) *m/z* calcd for $C_{20}H_{19}N_4O_2$ 347.1430; found 347.1511. HPLC*:* t_R = 20.92 min (purity = 96.4%).

*4.1.49. Methyl 6-((trimethylsilyl)ethynyl)picolinate (**52**).*

To a solution of methyl 6-bromopyridine-2-carboxylate **50** (1.0 g, 4.63 mmol) in THF (15 mL) were added dichlorobis(triphenylphosphine)palladium (0.163 mg, 0.23 mmol), CuI (88 mg, 0.46 mmol), Et_3N (15 mL) and ethynyltrimethylsilane (1.98 mL, 13.89 mmol). The stirred mixture was heated at 60 °C for 5 h, and then filtered on Celite®. The filtrate was concentrated under reduced pressure, and the residue was purified by silica gel chromatography 90/10 (petroleum ether/EtOAc) to afford **52** as a brown oil in 96% yield. ^{1}H NMR (300 MHz, $CDCl_3$) δ 8.06 (dd, *J* = 7.8, 1.1 Hz, 1H), 7.79 (t, *J* = 7.8 Hz, 1H), 7.62 (dd, *J* = 7.8, 1.1 Hz, 1H), 4.00 (s, 3H), 0.31 – 0.22 (m, 9H). ^{13}C NMR (75 MHz, $CDCl_3$) δ 165.3, 148.6, 143.4, 137.2, 130.7, 124.3, 102.9, 96.5, 53.1, -0.3. MS (ESI+): *m/z* (%): 234 (100) $[M+H]^+$.

*4.1.50. Methyl 6-ethynylpicolinate (**54**).*

To a solution of methyl 6-((trimethylsilyl)ethynyl)picolinate **52** (1.0 g, 4.23 mmol) in a mixture of CH_2Cl_2/MeOH (26 mL, 50:50, v/v) was added KF (0.74 g, 12.7 mmol). The mixture was stirred at room temperature overnight. The reaction mixture was filtered and concentrated *in*

vacuo. The residue was purified by flash chromatography on silica gel (petroleum ether/EtOAc, 80/20) to afford **54** (562 mg) as a brown solid in 82% yield. ^{1}H NMR (300 MHz, $CDCl_3$) δ 8.06 (dd, *J* = 7.8, 0.9 Hz, 1H), 7.80 (t, *J* = 7.8 Hz, 1H), 7.61 (dd, *J* = 7.8, 1.0 Hz, 1H), 3.97 (s, 3H), 3.18 (s, 1H). ^{13}C NMR (75 MHz, $CDCl_3$) δ 165.2, 148.5, 142.6, 137.4, 130.6, 124.7, 82.0, 78.6, 53.1. MS (ESI+): *m/z* (%): 162 (100) $[M+H]^+$.

*4.1.51. 6-Ethynylpicolinohydrazide (**56**).*

General procedure A was followed, using methyl ester **54** (550 mg, 3.41 mmol) to give **56** as an orange solid (550 mg) in 99% yield. ^{1}H NMR (300 MHz, $CDCl_3$) δ 8.94 (s, 1H), 8.14 (dd, *J* = 7.8, 1.1 Hz, 1H), 7.84 (t, *J* = 7.8 Hz, 1H), 7.61 (dd, *J* = 7.8, 1.1 Hz, 1H), 4.06 (s, 2H), 3.21 (s, 1H). ^{13}C NMR (75 MHz, $CDCl_3$) δ 163.9, 149.5, 141.2, 137.9, 130.2, 122.2, 82.1, 78.1. MS (ESI+): *m/z* (%): 162 (100) $[M+H]^+$.

*4.1.52. 6-Ethynylpicolinoyl azide (**58**).*

General procedure B was followed, using acyl hydrazine **56** (550 mg, 3.41 mmol), to give the desired acyl azide **58** (534 mg) as an off-white solid in 91% yield. ^{1}H NMR (300 MHz, $CDCl_3$) δ 8.11 (dd, *J* = 7.8, 0.9 Hz, 1H), 7.86 (t, *J* = 7.8 Hz, 1H), 7.69 (dd, *J* = 7.8, 0.9 Hz, 1H), 3.22 (s, 1H). ^{13}C NMR (75 MHz, $CDCl_3$) δ 171.5, 148.3, 142.7, 137.7, 131.6, 124.2, 81.7, 79.0. MS (ESI+): *m/z* (%): 172 (100) $[M+H]^+$.

*4.1.53. (±)-1-(6-ethynylpyridin-2-yl)-3-(6-oxo-1,2,3,4,6,10b-hexahydropyrido[2,1-a]isoindol-10-yl)urea (**(±)-60**).*

General procedure C was followed, using the acyl azide **58** (68 mg, 0.44 mmol) and tetrahydropyrido[2,1-*a*]isoindolone **(±)-24** (80 mg, 0.44 mmol). Purification by flash

chromatography using (CH_2Cl_2/MeOH/NH_4OH 96:4:1, v/v/v) gave the urea **(±)-60** (81 mg) as a white solid in 50% yield. ^{1}H NMR (300 MHz, DMSO) δ 10.64 (s, 1H), 10.06 (s, 1H), 8.17 (d, *J* = 7.5 Hz, 1H), 7.80 (t, *J* = 7.8 Hz, 1H), 7.51 – 7.37 (m, 3H), 7.24 (d, *J* = 7.3 Hz, 1H), 4.64 (d, *J* = 8.3 Hz, 1H), 4.55 (s, 1H), 4.27 (d, *J* = 10.3 Hz, 1H), 3.04 (t, *J* = 11.9 Hz, 1H), 2.63 (d, *J* = 11.6 Hz, 1H), 1.91 – 1.69 (m, 2H), 1.32 – 1.13 (m, 2H), 0.89 (dd, *J* = 25.0, 14.1 Hz, 1H). ^{13}C NMR (75 MHz, DMSO) δ 164.6, 152.9, 151.9, 139.5, 138.1, 135.2, 133.6, 132.9, 128.9, 122.8, 121.3, 117.7, 112.7, 82.7, 81.0, 57.1, 29.9, 25.1, 22.9. MS (ESI+): *m/z* (%): 347 (100) $[M+H]^+$. HRMS (ESI+) *m/z* calcd for $C_{20}H_{19}N_4O_2$ 347.1430; found 347.1510. HPLC: t_R = 25.30 min (purity = 97.7%).

4.1.54. (±)-1-(6-oxo-1,2,3,4,6,10b-hexahydropyrido[2,1-a]isoindol-10-yl)-3-(5-(1-(2-((1,2,3,4-tetrahydroacridin-9-yl)amino)ethyl)-1H-1,2,3-triazol-4-yl)pyridin-2-yl)urea ((±)-7).

General procedure D was followed, using the alkyne **(±)-59** (50 mg, 0.14 mmol) and azide **14** (37 mmg, 0.14 mmol). The purification by flash chromatography (CH_2Cl_2/MeOH/NH_4OH 97:3:1, v/v/v) gave the desired compound **(±)-7** as white off solid (65 mg) in 81% yield. ^{1}H NMR (300 MHz, DMSO) δ 9.34 (s, 1H), 8.64 (s, 1H), 8.55 – 8.51 (m, 3H), 8.45 (t, *J* = 2.2 Hz, 1H), 7.96 (dt, *J* = 8.8, 4.5 Hz, 2H), 7.70 (dd, *J* = 8.4, 0.9 Hz, 1H), 7.54 – 7.47 (m, 1H), 7.46 – 7.38 (m, 2H), 7.35 – 7.28 (m, 1H), 5.60 (t, *J* = 6.6 Hz, 1H), 4.64 (t, *J* = 6.0 Hz, 2H), 4.56 (dd, *J* = 11.5, 3.3 Hz, 1H), 4.26 (dd, *J* = 12.8, 4.0 Hz, 1H), 3.95 – 3.86 (m, 2H), 3.02 (dd, *J* = 12.8, 9.8 Hz, 1H), 2.87 (t, *J* = 6.1 Hz, 2H), 2.64 – 2.57 (m, 3H), 1.90 (d, *J* = 13.2 Hz, 1H), 1.83 – 1.72 (m, 5H), 1.63 (d, *J* = 13.4 Hz, 1H), 1.30 – 1.19 (m, 1H), 0.87 (qd, *J* = 12.7, 3.2 Hz, 1H). ^{13}C NMR (75 MHz, DMSO) δ 164.5, 158.0, 152.5, 149.3, 146.7, 143.2, 139.8, 139.2, 136.5, 135.8, 134.0, 133.0, 128.7, 128.3, 128.0, 126.63, 123.6, 123.5, 122.7, 122.7, 121.0, 120.4, 117.7, 117.1, 64.9,

57.6, 50.2, 47.5, 33.4, 29.8, 25.0, 24.9, 23.1, 22.6, 22.3. MS (ESI+): *m/z* (%) 614 (110) $[M+H]^+$. HRMS (ESI+) calcd for $C_{35}H_{36}N_9O_2$ 614.2914, found 614.2991. HPLC: t_R = 21.45 min (purity = 97.1%).

*4.1.55. (±)-1-(6-Oxo-1,2,3,4,6,10b-hexahydropyrido[2,1-a]isoindol-10-yl)-3-(6-(1-(2-((1,2,3,4-tetrahydroacridin-9-yl)amino)ethyl)-1H-1,2,3-triazol-4-yl)pyridin-2-yl)urea (**(±)-8**).*

The general procedure D was followed by using the alkyne (±)**-60** (45 mg, 0.13 mmol) and azide **14** (34 mg, 0.13 mmol). The purification by flash chromatography on silica gel (CH_2Cl_2/MeOH/NH_4OH 95:5:1, v/v/v) gave the desired compound **(±)-8** as yellow solid (68 mg) in 94% yield. ^{1}H NMR (300 MHz, DMSO) δ 10.52 (bs, 1H), 9.84 (s, 1H), 8.53 (s, 1H), 8.06 (dd, *J* = 7.4, 1.6 Hz, 1H), 7.93 (d, *J* = 8.4 Hz, 1H), 7.85 (t, *J* = 9.0 Hz 1H), 7.69 (d, *J* = 7.8 Hz, 1H), 7.53 – 7.37 (m, 5H), 7.29 (ddd, *J* = 8.1, 6.9, 1.1 Hz, 1H), 5.59 (t, *J* = 6.5 Hz, 1H), 4.84 (dd, *J* = 11.3, 3.3 Hz, 1H), 4.68 (t, *J* = 6.0 Hz, 2H), 4.20 (d, *J* = 12.1 Hz, 1H), 3.91 (dd, *J* = 12.6, 6.5 Hz, 2H), 2.94 – 2.81 (m, 3H), 2.61 (t, *J* = 5.8 Hz, 2H), 2.43 (d, *J* = 10.5 Hz, 1H), 1.83 – 1.58 (m, 6H), 1.23 – 1.10 (m, 2H), 0.78 (dd, *J* = 23.6, 12.0 Hz, 1H). ^{13}C NMR (75 MHz, DMSO) δ 164.5, 158.0, 152.7, 152.1, 149.3, 147.1, 146.7, 146.0, 139.6, 135.9, 133.6, 133.0, 128.6, 128.3, 126.0, 124.0, 123.8, 123.5, 122.7, 120.4, 117.8, 117.1, 114.1, 111.1, 57.1, 54.9, 50.1, 47.6, 33.4, 29.5, 25.0, 24.9, 22.6, 22.6, 22.3. MS (ESI+): *m/z* (%): 614 (100) $[M+H]^+$. HRMS (ESI+) *m/z* calcd for $C_{35}H_{36}N_9O_2$ 614.2914; found 614.2989. HPLC: t_R = 22.87 min (purity = 97.5%).

4.2. Evaluation of the inhibitory activity toward human AChE and BChE from human serum

The capacity of tested compounds to inhibit AChE and BChE activity was assessed by following the Ellman's method.[66] The assay was performed at 37 °C with a Jasco V-530

double beam Spectrophotometer (Jasco Europe). A stock solution of AChE was prepared by dissolving human recombinant AChE (Sigma Aldrich, Italy) lyophilized powder in 0.1 M phosphate buffer (pH = 8.0) containing Triton X-100 0.1%. A stock solution of BChE from human serum (Sigma Aldrich, Italy) was prepared by dissolving the lyophilized powder in an aqueous solution of gelatine 0.1%. Stock solutions of inhibitors (1 or 2 mM) were prepared in methanol. Five increasing concentrations of the inhibitor were used, able to give an inhibition of the enzymatic activity in the range of 20-80%. The assay solution consisted of a 0.1 M phosphate buffer pH 8.0, with the addition of 340 mM DTNB, 0.02 unit/mL of human recombinant AChE, or BChE from human serum and 550 µM of substrate (ATCh or BTCh, respectively). 50 µL aliquots of increasing concentration of the tested compound were added to the assay solution and preincubated for 20 min at 37 °C with the enzyme, followed by the addition of substrate. Upon substrate addition the increase in the absorbance at 412 nm was monitored for 3 min. Assays were carried out with a blank containing all components except AChE or BChE in order to account for the non-enzymatic reaction. The reaction rates were compared and the percent inhibition due to the presence of tested inhibitor at increasing concentration was calculated. Each concentration was analyzed in triplicate, and IC_{50} values were determined graphically from log concentration–inhibition curves (GraphPad Prism 4.03 software, GraphPad Software Inc.). Each IC_{50} value was determined from at least two independent experiments each performed in triplicate.

4.3. Kinase assays

CDK5/p25 (human, recombinant) kinase activity was assayed in buffer B (60 mM ß-glycerophosphate, 30 mM p-nitrophenylphosphate, 25 mM Mops (pH 7.2), 5 mM EGTA, 15 mM $MgCl_2$, 1 mM DTT, 0.1 mM sodium vanadate, 1 mM phenylphosphate), with 1 µg of

histone H1/μL as substrate. GSK-3α/β (porcine brain, native) was assayed in buffer A (10 mM $MgCl_2$, 1 mM EGTA, 1 mM DTT, 25 mM Tris-HCl pH 7.5, 50 μg heparin/mL) using a GSK-3 specific substrate (GS-1: YRRAAVPPSPSLSRHSSPHQ-pSEDEEE) (Proteogenix, Oberhausbergen, France). Kinase activities were assayed at 30 °C, at a final ATP concentration of 15 μM in the presence of 15 μM [γ-33P] ATP (3,000 Ci/mmol; 10 mCi/mL) in a final volume of 30 μL. After 30 min incubation at 30°C, the reaction was stopped by harvesting onto P81 phosphocellulose papers (Whatman) using a FilterMate harvester (Packard) and were washed in 1% phosphoric acid. Scintillation fluid was added and the radioactivity measured in a Packard counter. Blank values were subtracted and activities expressed in percent of the maximum activity, i.e., in the absence of inhibitors.

4.4. Cytotoxicity assays

4.4.1. Cell culture

HuH7, Caco-2, MDA-MB-231, HCT116, PC3, MCF7 and NCI-H727 cancer cell lines were obtained from the ECACC collection (Porton Down, UK). Cells were grown at 37 °C, 5% CO_2 in ECACC recommended media: DMEM for HuH7 and MDA-MB-231, EMEM for MCF7 and CaCo-2, McCoy's for HCT116 and RPMI for PC3 and NCI-H727. All culture media were supplemented by 10% of FBS, 1% of penicillin-streptomycin and 2 mM glutamine.

The human neuroblastoma cell line SH-SY5Y and the Madin-Darby Canine Kidney (MDCK) cells retrovirally transfected with the human MDR1 cDNA (MDCKII-MDR1) were cultured in DMEM supplemented with 100 U/ml penicillin, 100 μg/mL streptomycin and 10% (v/v) heat-inactivated Fetal Bovine Serum (FBS). All cells were grown at 37 ºC in a humidified atmosphere with 5% CO_2. All materials for cell culturing were purchased from EuroClone, Italy.

4.4.2. Cytotoxic assay

Chemicals were solubilized in DMSO at a concentration of 10 mM (stock solution) and diluted in culture medium to the desired final concentrations. The dose effect cytotoxic assays (IC_{50} determination) were performed by increasing the concentration of each chemical (final well concentrations: 0.1 – 0.3 – 0.9 – 3.0 – 9.0 – 25 μM). The cells were plated in 96-well plates (4000 cells/well). Twenty-four hours after seeding, the cells were exposed to chemicals. After 48 h of treatment, the cells were washed in PBS and fixed in cooled 90% ethanol/5% acetic acid for 20 minutes and the nuclei are stained with Hoechst 33342 (B2261 Sigma). Image acquisition and analysis are performed using a Cellomics ArrayScan VTI/HCS Reader (ThermoScientific). The survival percentages were calculated as the percentage of cell number after compound treatment over cell number after DMSO treatment. The concentrations of each drug responsible for 50% inhibition of cell growth (IC_{50}) were calculated in Microsoft Excel.

Cell growth of SH-SY5Y cells after incubation with compounds for 24 h and 72 h was determined using the 3-[4,5-dimethylthiazol-2-yl]-2,5-diphenyltetrazoliumbromide (MTT) assay according to the protocol previously described.[67, 68] Cells were seeded in 96-well plates at a density of $5x10^3$ cells/well. The attached cells were then exposed to various concentrations of drugs in the range 0.1-100 μM. The effect of compounds on the proliferation of SHSY5Y cells after 24 h of incubation was expressed as % cell viability at the highest tested dose (100 μM). The concentrations of each drug responsible for 50% inhibition of cell growth (IC_{50}) after 72 h of incubation were calculated from dose-response curves using nonlinear multipurpose curve fitting program GraphPad Prism 5.0. Each experiment was performed in triplicate. The viability of

MDCKII-MDR1 cells after treatment for 2 h with compounds at a concentration of 75 µM was also evaluated in order to avoid interference with cell viability during the permeability assay.

4.5. Bi-directional transport studies

MDCKII-MDR1 cells were used to mimic *in vitro* the blood brain barrier (BBB). The BBB penetration of compounds was evaluated according to the protocol previously described.[67-69] Cell monolayers were grown on 24-well Transwell® insert (diameter 6.5 mm, pore size 0.4 µm, apical volume 0.1 mL, basolateral volume 0.6 mL) and the formation of confluent MDCKII-MDR1 monolayers with tight junctions was confirmed by microscopy and TEER values. Cell monolayers with TEER values of 800 Ohm.cm^2 were used for the transport experiments. Diazepam and FD4 (fluorescein isothiocyanate-dextran) were used as markers for the transcellular and paracellular pathway, respectively, and as an internal control to verify tight junction integrity during the assay.

The apparent permeability (P_{app} AP and BL in cm/sec), was calculated according to the following equation:

$$P_{app} = \left(\frac{Va}{area \times time}\right) \times \left(\frac{[Drug]_{acceptor}}{[Drug]_{initial}}\right)$$

"Va"= volume in the acceptor well,
"area" = surface area of the membrane,
"time"= total transport time,
"$[drug]_{acceptor}$" = concentration of the drug in the acceptor chamber;
"$[drug]_{initial}$" = initial drug concentration in the AP or BL chamber;
The efflux ratio (ER) was calculated using the following equation:

$$ER = \frac{P_{app}, BL - AP}{P_{app}, AP - BL}$$

Papp, BL-AP: apparent permeability of basal-to-apical transport;
Papp, AP-BL: apparent permeability of apical-to-basal transport.
An efflux ratio greater than 2 indicates that a test compound is likely to be a substrate for P-gp transport.

4.6. Molecular docking

The crystal structure of the mouse AChE-*anti*-TZ2-PA6 complex (PDB code 1Q84) was used for molecular docking.[50] Docking calculations were carried out using Autodock Vina.[57] MTDL structures were created and minimized using the MMFF94 force field implanted in ChemBio3D Ultra 12.0 (PerkinElmer, Inc. Waltham, MA, USA). MTDL and mouse AChE were further prepared using Autodock Tools 1.5.6.[70] Structural water molecules were conserved in the model in order to improve docking accuracy. Residues in the active site of AChE (Tyr 72, Tyr 286, Tyr 341, Tyr 124, Tyr 337, Trp 86) were selected as flexible. The 3D affinity grid box was designed to include the full active-site gorge of AChE. Docking calculations were performed using the default parameter set of AutoDock Vina to generate nine docking poses per molecule. Vina generated the estimated total Gibbs free energy of binding in kcal/mol, which could be converted to the apparent constant, K_i, using the relationship $\Delta G=RT.\ln(K_i)$. Docking poses were visualized using the PyMOL molecular graphics system.[71]

The crystal structure of GSK-3β in complex with PF-04802367 (PBD code 5K5N) was used for molecular docking.[58] Docking calculations were performed using the same protocol as for AChE.

4.7. Crystallization and structure determination

Purified *Tc*AChE (12 mg mL^{-1}) was obtained as described by Sussman *et al.*[72] Crystals were grown by the hanging-drop vapor diffusion method at 4 °C for 2-3 weeks. Drops of 2 µl were produced by mixing an equal volume of protein solution with 30% PEG 200/50 mM MES, pH 6.0. Crystals were then harvested and soaked in the above-mentioned mother liquor, complemented with candidate compounds at a concentration of 1 mM, for at least 12 h. Diffraction data were collected on the ID23eh2 (for compounds **2** and **3**) and ID30A1 (for compound **6**) beamlines at the European Synchrotron Radiation Facility (ESRF, Grenoble, France). Crystals were flash-frozen and stored in liquid nitrogen until used for data collection.

Diffraction images were indexed and integrated using XDS,[73] and intensities were further scaled and merged with XSCALE. Phases were retrieved using the molecular replacement technique with PHASER[74] using PDB entry 2XI4 as the starting model. All data were collected from orthorhombic *Tc*AChE crystals, and two subunits were placed in the asymmetric unit. The model was refined by iterative cycles of refinement with phenix.refine[75] and model building using Coot.[76] With phenix.refine, refinement of atomic positions (both in real and reciprocal space) and individual isotropic temperature factors was performed. All ligand topologies were generated with the PRODRG server,[77] and their occupancies were refined during the final cycles of refinement. The coordinates and structure factors have been deposited in the Protein Data Bank under accession codes 6H12, 6H13, 6H14, for complexes of *Tc*AChE with **2**, **3**, and **6**, respectively. Data collection and refinement statistics are detailed in supporting information.

Acknowledgments

Labex SynOrg (ANR-11-LABX-0029) is acknowledged for a PhD fellowship to K. O. and the Agence Nationale de la Recherche (ANR) (project MultiClick, grant number ANR-12-BS07-008-01) for financial support. This work was also partially supported by the INSA Rouen, Rouen Normandy University, the Centre National de la Recherche Scientifique (CNRS) and the Region Normandie (CRUNCh network).

Appendix A. Supplementary data

Supplementary data include docking poses, procedures for the preparation of azides **34A-C**, ^{1}H NMR and ^{13}C NMR spectra, HPLC purity analyses of MTDLs **2**, **3**, **4**, **6**, **7** and **8**, supplementary figures of crystallographic models, data collection and refinement statistics and kinase selectivity assays.

References

[1] M. Prince, A. Wimo, M. Guerchet, G.-C. Ali, Y.-T. Wu, M. Prina, World Alzheimer Report 2015: the global impact of dementia: an analysis of prevalence, incidence, cost and trends, Alzheimer's Disease International, London, 2015.

[2] I.W. Hamley, The amyloid beta peptide: a chemist's perspective. Role in Alzheimer's and fibrillization, Chem. Rev., 112 (2012) 5147-5192.

[3] M.A. Meraz-Rios, K.I. Lira-De Leon, V. Campos-Pena, M.A. De Anda-Hernandez, R. Mena-Lopez, Tau oligomers and aggregation in Alzheimer's disease, J. Neurochem., 112 (2010) 1353-1367.

[4] H.W. Querfurth , F.M. LaFerla Alzheimer's Disease, New Engl. J. Med., 362 (2010) 329-344.

[5] D.A. Smith, Treatment of Alzheimer's disease in the long-term-care setting, Am. J. Health Syst. Pharm., 66 (2009) 899-907.

[6] G.T. Grossberg, V. Pejovic, M.L. Miller, S.M. Graham, Memantine therapy of behavioral symptoms in community-dwelling patients with moderate to severe Alzheimer's disease, Dement. Geriatr. Cogn. Disord., 27 (2009) 164-172.

[7] D. Wilkinson, Y. Wirth, C. Goebel, Memantine in patients with moderate to severe Alzheimer's disease: meta-analyses using realistic definitions of response, Dement. Geriatr. Cogn. Disord., 37 (2014) 71-85.

[8] D.J. Findlay, P.J. Connelly, Memantine (Ebixa) in the later stages of dementia, Hosp. Med., 64 (2003) 654-657.

[9] R.R. Tampi, C.H. van Dyck, Memantine: efficacy and safety in mild-to-severe Alzheimer’s disease, Neuropsychiatr. Dis. Treat., 3 (2007) 245-258.

[10] J.L. Cummings, T. Morstorf, K. Zhong, Alzheimer’s disease drug-development pipeline: few candidates, frequent failures, Alzheimers Res. Ther., 6 (2014) 37.

[11] S.O. Bachurin, E.V. Bovina, A.A. Ustyugov, Drugs in Clinical Trials for Alzheimer's Disease: The Major Trends, Med. Res. Rev., 37 (2017) 1186-1225.

[12] J. Godyń, J. Jończyk, D. Panek, B. Malawska, Therapeutic strategies for Alzheimer's disease in clinical trials, Pharmacol. Rep., 68 (2016) 127-138.

[13] P. Talwar, J. Sinha, S. Grover, C. Rawat, S. Kushwaha, R. Agarwal, V. Taneja, R. Kukreti, Dissecting Complex and Multifactorial Nature of Alzheimer's Disease Pathogenesis: a Clinical, Genomic, and Systems Biology Perspective, Mol. Neurobiol., 53 (2016) 4833-4864.

[14] M. Bajda, N. Guzior, M. Ignasik, B. Malawska, Multi-target-directed ligands in Alzheimer's disease treatment, Curr. Med. Chem., 18 (2011) 4949-4975.

[15] A. Cavalli, M.L. Bolognesi, A. Minarini, M. Rosini, V. Tumiatti, M. Recanatini, C. Melchiorre, Multi-target-directed ligands to combat neurodegenerative diseases, J. Med. Chem., 51 (2008) 347-372.

[16] N. Guzior, A. Wieckowska, D. Panek, B. Malawska, Recent development of multifunctional agents as potential drug candidates for the treatment of Alzheimer's disease, Curr. Med. Chem., 22 (2015) 373-404.

[17] R. Morphy, Z. Rankovic, Designed multiple ligands. An emerging drug discovery paradigm, J. Med. Chem., 48 (2005) 6523-6543.

[18] M. Rosini, V. Andrisano, M. Bartolini, M.L. Bolognesi, P. Hrelia, A. Minarini, A. Tarozzi, C. Melchiorre, Rational approach to discover multipotent anti-Alzheimer drugs, J. Med. Chem., 48 (2005) 360-363.

[19] S. Das, S. Basu, Multi-targeting Strategies for Alzheimer's Disease Therapeutics: Pros and Cons, Curr. Top. Med. Chem., 17 (2017) 3017-3061.

[20] M.J. Oset-Gasque, J. Marco-Contelles, Alzheimer's Disease, the "One-Molecule, One-Target" Paradigm, and the Multitarget Directed Ligand Approach, ACS Chem. Neurosci., 9 (2018) 401-403.

[21] M.C. Carreiras, E. Mendes, M.J. Perry, A.P. Francisco, J. Marco-Contelles, The Multifactorial Nature of Alzheimer Disease for Developing Potential Therapeutics, Curr. Top. Med. Chem., 13 (2013) 1745-1770.

[22] I. Gulcin, M. Abbasova, P. Taslimi, Z. Huyut, L. Safarova, A. Sujayev, V. Farzaliyev, S. Beydemir, S.H. Alwasel, C.T. Supuran, Synthesis and biological evaluation of aminomethyl and alkoxymethyl derivatives as carbonic anhydrase, acetylcholinesterase and butyrylcholinesterase inhibitors, J. Enzyme Inhib. Med. Chem., 32 (2017) 1174-1182.

[23] A. Talevi, Multi-target pharmacology: possibilities and limitations of the "skeleton key approach" from a medicinal chemist perspective, Front. Pharmacol., 6 (2015) 205.

[24] M.J. Savage, D.E. Gingrich, Advances in the development of kinase inhibitor therapeutics for Alzheimer's disease, Drug Dev. Res., 70 (2009) 125-144.

[25] L. Martin, X. Latypova, C.M. Wilson, A. Magnaudeix, M.L. Perrin, C. Yardin, F. Terro, Tau protein kinases: involvement in Alzheimer's disease, Ageing Res Rev, 12 (2013) 289-309.

[26] D.P. Hanger, B.H. Anderton, W. Noble, Tau phosphorylation: the therapeutic challenge for neurodegenerative disease, Trends Mol. Med., 15 (2009) 112-119.

[27] S.L. Liu, C. Wang, T. Jiang, L. Tan, A. Xing, J.T. Yu, The Role of Cdk5 in Alzheimer's Disease, Mol. Neurobiol., 53 (2016) 4328-4342.

[28] D.E. Hurtado, L. Molina-Porcel, J.C. Carroll, C. Macdonald, A.K. Aboagye, J.Q. Trojanowski, V.M. Lee, Selectively silencing GSK-3 isoforms reduces plaques and tangles in mouse models of Alzheimer's disease, J. Neurosci., 32 (2012) 7392-7402.

[29] C.J. Phiel, C.A. Wilson, V.M. Lee, P.S. Klein, GSK-3alpha regulates production of Alzheimer's disease amyloid-beta peptides, Nature, 423 (2003) 435-439.

[30] A. Martinez, D.I. Perez, C. Gil, Lessons learnt from glycogen synthase kinase 3 inhibitors development for Alzheimer's disease, Curr. Top. Med. Chem., 13 (2013) 1808-1819.

[31] A. Martinez, C. Gil, D.I. Perez, Glycogen Synthase Kinase 3 Inhibitors in the Next Horizon for Alzheimer's Disease Treatment, Int. J. Alzheimers Dis., 2011 (2011) 280502.

[32] L. Avrahami, D. Farfara, M. Shaham-Kol, R. Vassar, D. Frenkel, H. Eldar-Finkelman, Inhibition of glycogen synthase kinase-3 ameliorates beta-amyloid pathology and restores lysosomal acidification and mammalian target of rapamycin activity in the Alzheimer disease mouse model: in vivo and in vitro studies, J. Biol. Chem., 288 (2013) 1295-1306.

[33] M.-Y. Noh, K. Chun, B.Y. Kang, H. Kim, J.-S. Park, H.-C. Lee, Y.-H. Kim, S. Ku, S.H. Kim, Newly developed glycogen synthase kinase-3 (GSK-3) inhibitors protect neuronal cells death in amyloid-beta induced cell model and in a transgenic mouse model of Alzheimer’s disease, Biochem. Biophys. Res. Commun., 435 (2013) 274-281.

[34] J.A. Morales-Garcia, R. Luna-Medina, S. Alonso-Gil, M. Sanz-SanCristobal, V. Palomo, C. Gil, A. Santos, A. Martinez, A. Perez-Castillo, Glycogen Synthase Kinase 3 Inhibition Promotes Adult Hippocampal Neurogenesis in Vitro and in Vivo, ACS Chem. Neurosci., 3 (2012) 963-971.

[35] T. Kramer, B. Schmidt, F. Lo Monte, Small-Molecule Inhibitors of GSK-3: Structural Insights and Their Application to Alzheimer's Disease Models, Int. J. Alzheimers Dis., 2012 (2012) 381029.

[36] N.C. Inestrosa, M.C. Dinamarca, A. Alvarez, Amyloid-cholinesterase interactions. Implications for Alzheimer's disease, FEBS J., 275 (2008) 625-632.

[37] A. Alvarez, C. Opazo, R. Alarcon, J. Garrido, N.C. Inestrosa, Acetylcholinesterase promotes the aggregation of amyloid-beta-peptide fragments by forming a complex with the growing fibrils, J. Mol. Biol., 272 (1997) 348-361.

[38] F.J. Carvajal, N.C. Inestrosa, Interactions of AChE with Aβ Aggregates in Alzheimer's Brain: Therapeutic Relevance of IDN 5706, Front. Mol. Neurosci., 4 (2011) 19.

[39] N.C. Inestrosa, A. Alvarez, C.A. Perez, R.D. Moreno, M. Vicente, C. Linker, O.I. Casanueva, C. Soto, J. Garrido, Acetylcholinesterase accelerates assembly of amyloid-beta-peptides into Alzheimer's fibrils: possible role of the peripheral site of the enzyme, Neuron, 16 (1996) 881-891.

[40] A. Minarini, A. Milelli, E. Simoni, M. Rosini, M.L. Bolognesi, C. Marchetti, V. Tumiatti, Multifunctional Tacrine Derivatives in Alzheimer's Disease, Curr. Top. Med. Chem., 13 (2013) 1771-1786.

[41] A. Milelli, A. De Simone, N. Ticchi, H.H. Chen, N. Betari, V. Andrisano, V. Tumiatti, Tacrine-based Multifunctional Agents in Alzheimer's Disease: An Old Story in Continuous Development, Curr. Med. Chem., 24 (2017) 3522-3546.

[42] D. Toiber, A. Berson, D. Greenberg, N. Melamed-Book, S. Diamant, H. Soreq, N-acetylcholinesterase-induced apoptosis in Alzheimer's disease, PLoS One, 3 (2008) e3108.

[43] H. Lin, Q. Li, K. Gu, J. Zhu, X. Jiang, Y. Chen, H. Sun, Therapeutic Agents in Alzheimer's Disease Through a Multi-targetdirected Ligands Strategy: Recent Progress Based on Tacrine Core, Curr. Top. Med. Chem., 17 (2017) 3000-3016.

[44] B. Sameem, M. Saeedi, M. Mahdavi, A. Shafiee, A review on tacrine-based scaffolds as multi-target drugs (MTDLs) for Alzheimer's disease, Eur. J. Med. Chem., 128 (2017) 332-345.

[45] K. Spilovska, J. Korabecny, E. Nepovimova, R. Dolezal, E. Mezeiova, O. Soukup, K. Kuca, Multitarget Tacrine Hybrids with Neuroprotective Properties to Confront Alzheimer's Disease, Curr. Top. Med. Chem., 17 (2017) 1006-1026.

[46] X.-Y. Jiang, T.-K. Chen, J.-T. Zhou, S.-Y. He, H.-Y. Yang, Y. Chen, W. Qu, F. Feng, H.-P. Sun, Dual GSK-3β/AChE Inhibitors as a New Strategy for Multitargeting Anti-Alzheimer’s Disease Drug Discovery, ACS Med. Chem. Lett., 9 (2018) 171-176.

[47] H. Eldar-Finkelman, A. Martinez, GSK-3 Inhibitors: Preclinical and Clinical Focus on CNS, Front. Mol. Neurosci., 4 (2011) 32.

[48] R. Boulahjar, A. Ouach, S. Bourg, P. Bonnet, O. Lozach, L. Meijer, C. Guguen-Guillouzo, R. Le Guevel, S. Lazar, M. Akssira, Y. Troin, G. Guillaumet, S. Routier, Advances in tetrahydropyrido[1,2-a]isoindolone (valmerins) series: Potent glycogen synthase kinase 3 and cyclin dependent kinase 5 inhibitors, Eur. J. Med. Chem., 101 (2015) 274-287.

[49] R. Boulahjar, A. Ouach, C. Matteo, S. Bourg, M. Ravache, R. le Guevel, S. Marionneau, T. Oullier, O. Lozach, L. Meijer, C. Guguen-Guillouzo, S. Lazar, M. Akssira, Y. Troin, G. Guillaumet, S. Routier, Novel tetrahydropyrido[1,2-a]isoindolone derivatives (valmerins): potent cyclin-dependent kinase/glycogen synthase kinase 3 inhibitors with antiproliferative activities and antitumor effects in human tumor xenografts, J. Med. Chem., 55 (2012) 9589-9606.

[50] Y. Bourne, H.C. Kolb, Z. Radic, K.B. Sharpless, P. Taylor, P. Marchot, Freeze-frame inhibitor captures acetylcholinesterase in a unique conformation, Proc. Natl. Acad. Sci. U. S. A., 101 (2004) 1449-1454.

[51] A. Krasinski, Z. Radic, R. Manetsch, J. Raushel, P. Taylor, K.B. Sharpless, H.C. Kolb, In situ selection of lead compounds by click chemistry: target-guided optimization of acetylcholinesterase inhibitors, J. Am. Chem. Soc., 127 (2005) 6686-6692.

[52] W.G. Lewis, L.G. Green, F. Grynszpan, Z. Radic, P.R. Carlier, P. Taylor, M.G. Finn, K.B. Sharpless, Click chemistry in situ: acetylcholinesterase as a reaction vessel for the selective assembly of a femtomolar inhibitor from an array of building blocks, Angew. Chem. Int. Ed., 41 (2002) 1053-1057.

[53] Y. Bourne, Z. Radic, H.C. Kolb, K.B. Sharpless, P. Taylor, P. Marchot, Structural insights into conformational flexibility at the peripheral site and within the active center gorge of AChE, Chem. Biol. Interact., 157-158 (2005) 159-165.

[54] J.P. Colletier, B. Sanson, F. Nachon, E. Gabellieri, C. Fattorusso, G. Campiani, M. Weik, Conformational flexibility in the peripheral site of Torpedo californica acetylcholinesterase

revealed by the complex structure with a bifunctional inhibitor, J. Am. Chem. Soc., 128 (2006) 4526-4527.

[55] E.H. Rydberg, B. Brumshtein, H.M. Greenblatt, D.M. Wong, D. Shaya, L.D. Williams, P.R. Carlier, Y.P. Pang, I. Silman, J.L. Sussman, Complexes of alkylene-linked tacrine dimers with Torpedo californica acetylcholinesterase: Binding of Bis5-tacrine produces a dramatic rearrangement in the active-site gorge, J. Med. Chem., 49 (2006) 5491-5500.

[56] A. Ouach, R. Boulahjar, C. Vala, S. Bourg, P. Bonnet, C. Guguen-Guillouzo, M. Ravache, R. Le Guevel, O. Lozach, S. Lazar, Y. Troin, L. Meijer, S. Ruchaud, M. Akssira, G. Guillaumet, S. Routier, Novel optimization of valmerins (tetrahydropyrido[1,2-a]isoindolones) as potent dual CDK5/GSK3 inhibitors, Eur. J. Med. Chem., 115 (2016) 311-325.

[57] O. Trott, A.J. Olson, AutoDock Vina: improving the speed and accuracy of docking with a new scoring function, efficient optimization, and multithreading, J. Comput. Chem., 31 (2010) 455-461.

[58] S.H. Liang, J.M. Chen, M.D. Normandin, J.S. Chang, G.C. Chang, C.K. Taylor, P. Trapa, M.S. Plummer, K.S. Para, E.L. Conn, L. Lopresti-Morrow, L.F. Lanyon, J.M. Cook, K.E.G. Richter, C.E. Nolan, J.B. Schachter, F. Janat, Y. Che, V. Shanmugasundaram, B.A. Lefker, B.E. Enerson, E. Livni, L. Wang, N.J. Guehl, D. Patnaik, F.F. Wagner, R. Perlis, E.B. Holson, S.J. Haggarty, G.E. Fakhri, R.G. Kurumbail, N. Vasdev, Discovery of a Highly Selective Glycogen Synthase Kinase-3 Inhibitor (PF-04802367) That Modulates Tau Phosphorylation in the Brain: Translation for PET Neuroimaging, Angew. Chem. Int. Ed., 55 (2016) 9601-9605.

[59] R. Boulahjar, A. Ouach, C. Matteo, S. Bourg, M. Ravache, R.l. Guével, S. Marionneau, T. Oullier, O. Lozach, L. Meijer, C. Guguen-Guillouzo, S. Lazar, M. Akssira, Y. Troin, G. Guillaumet, S. Routier, Novel Tetrahydropyrido[1,2-a]isoindolone Derivatives (Valmerins): Potent Cyclin-Dependent Kinase/Glycogen Synthase Kinase 3 Inhibitors with Antiproliferative Activities and Antitumor Effects in Human Tumor Xenografts, J. Med. Chem., 55 (2012) 9589-9606.

[60] K. Oukoloff, F. Buron, S. Routier, L. Jean, P.Y. Renard, Synthetic Route to Rare Isoindolones Derivatives, Eur. J. Org. Chem., (2015) 2450-2456.

[61] X. Yang, W. Wedajo, Y. Yamada, S.-L. Dahlroth, J.J.-L. Neo, T. Dick, W.-K. Chui, 1,3,5-triazaspiro[5.5]undeca-2,4-dienes as selective Mycobacterium tuberculosis dihydrofolate reductase inhibitors with potent whole cell activity, Eur. J. Med. Chem., 144 (2018) 262-276.

[62] A. Nordberg, C. Ballard, R. Bullock, T. Darreh-Shori, M. Somogyi, A review of butyrylcholinesterase as a therapeutic target in the treatment of Alzheimer's disease, Prim. Care Companion CNS Disord., 15 (2013).

[63] A. Lopalco, H. Ali, N. Denora, E. Rytting, Oxcarbazepine-loaded polymeric nanoparticles: development and permeability studies across in vitro models of the blood-brain barrier and human placental trophoblast, International journal of nanomedicine, 10 (2015) 1985-1996.

[64] T. Cassano, A. Lopalco, M. de Candia, V. Laquintana, A. Lopedota, A. Cutrignelli, M. Perrone, R.M. Iacobazzi, G. Bedse, M. Franco, N. Denora, C.D. Altomare, Oxazepam–Dopamine Conjugates Increase Dopamine Delivery into Striatum of Intact Rats, Mol. Pharm., 14 (2017) 3178-3187.

[65] S. Salentin, S. Schreiber, V.J. Haupt, M.F. Adasme, M. Schroeder, PLIP: fully automated protein-ligand interaction profiler, Nucleic Acids Res., 43 (2015) W443-447.

[66] G.L. Ellman, K.D. Courtney, V. Andres, Jr., R.M. Featherstone, A new and rapid colorimetric determination of acetylcholinesterase activity, Biochem. Pharmacol., 7 (1961) 88-95.

[67] L. Pisani, R. Farina, R. Soto-Otero, N. Denora, G.F. Mangiatordi, O. Nicolotti, E. Mendez-Alvarez, C.D. Altomare, M. Catto, A. Carotti, Searching for Multi-Targeting Neurotherapeutics against Alzheimer's: Discovery of Potent AChE-MAO B Inhibitors through the Decoration of the 2H-Chromen-2-one Structural Motif, Molecules, 21 (2016) 362.

[68] S. Franchini, L.I. Manasieva, C. Sorbi, U.M. Battisti, P. Fossa, E. Cichero, N. Denora, R.M. Iacobazzi, A. Cilia, L. Pirona, S. Ronsisvalle, G. Aricò, L. Brasili, Synthesis, biological evaluation and molecular modeling of 1-oxa-4-thiaspiro- and 1,4-dithiaspiro[4.5]decane derivatives as potent and selective 5-HT1A receptor agonists, Eur. J. Med. Chem., 125 (2017) 435-452.

[69] N. Denora, V. Laquintana, A. Lopedota, M. Serra, L. Dazzi, G. Biggio, D. Pal, A.K. Mitra, A. Latrofa, G. Trapani, G. Liso, Novel L-Dopa and dopamine prodrugs containing a 2-phenyl-imidazopyridine moiety, Pharm. Res., 24 (2007) 1309-1324.

[70] M.F. Sanner, Python: a programming language for software integration and development, J. Mol. Graph. Model., 17 (1999) 57-61.

[71] W.L. DeLano, The PyMOL Molecular Graphics System, in, 2002.

[72] J.L. Sussman, M. Harel, F. Frolow, L. Varon, L. Toker, A.H. Futerman, I. Silman, Purification and crystallization of a dimeric form of acetylcholinesterase from Torpedo californica subsequent to solubilization with phosphatidylinositol-specific phospholipase C, J. Mol. Biol., 203 (1988) 821-823.

[73] W. Kabsch, Integration, scaling, space-group assignment and post-refinement, Acta Crystallogr. D Biol. Crystallogr., 66 (2010) 133-144.

[74] A.J. McCoy, R.W. Grosse-Kunstleve, P.D. Adams, M.D. Winn, L.C. Storoni, R.J. Read, Phaser crystallographic software, J. Appl. Crystallogr., 40 (2007) 658-674.

[75] P.V. Afonine, M. Mustyakimov, R.W. Grosse-Kunstleve, N.W. Moriarty, P. Langan, P.D. Adams, Joint X-ray and neutron refinement with phenix.refine, Acta Crystallogr. D Biol. Crystallogr., 66 (2010) 1153-1163.

[76] P. Emsley, B. Lohkamp, W.G. Scott, K. Cowtan, Features and development of Coot, Acta Crystallogr. D Biol. Crystallogr., 66 (2010) 486-501.

[77] A.W. Schuttelkopf, D.M. van Aalten, PRODRG: a tool for high-throughput crystallography of protein-ligand complexes, Acta Crystallogr. D Biol. Crystallogr., 60 (2004) 1355-1363.